Spring 2008

Numerical Simulations of a Nonlinear Transmission Line

Stuart Rogers
Old Dominion University

NUMERICAL SIMULATIONS OF A NONLINEAR TRANSMISSION LINE

by

Stuart Rogers
Sc.M. May 2004, Brown University, Providence, RI

A Thesis Submitted to the Faculty of
Old Dominion University in Partial Fulfillment of the
Requirement for the Degree of

MASTER OF SCIENCE

ELECTRICAL ENGINEERING

OLD DOMINION UNIVERSITY
May 2008

Approved by:

Ravindra P. Joshi (Director)

Juergen Kolb (Member)

Linda L. Vahala (Member)

ABSTRACT

NUMERICAL SIMULATIONS OF A NONLINEAR TRANSMISSION LINE

Stuart Rogers
Old Dominion University, 2008
Director: Dr. Ravindra P. Joshi

This thesis investigates wave propagation along a nonlinear transmission line having a voltage-dependent capacitance. The telegrapher's equations that model wave propagation along such a transmission line are derived and shown to represent a nonlinear hyperbolic system of balance laws. The Lax-Friedrichs, Lax-Wendroff, and hybrid numerical schemes for obtaining approximate solutions to nonlinear hyperbolic systems of balance laws are presented, analyzed, and applied to the nonlinear telegrapher's equations. The Lax-Wendroff and hybrid schemes are invoked to numerically simulate wave propagation along a nonlinear transmission line. Simulations obtained via the hybrid scheme are used to briefly study the potential application of a nonlinear transmission line as a pulse generator.

Since they may generate ultra short (nanosecond) rise time voltage waveforms, nonlinear transmission lines could have applicability to pulsed power systems and high power microwaves. Moreover, short duration, high intensity voltage pulses have been demonstrated to penetrate biological cells and affect the internal organelles. Thus, such voltage shaping could provide the technological tools for intracellular manipulation and several potential biomedical engineering applications.

Though only one particular voltage-dependent capacitance was selected for the nonlinear transmission line analysis, the method described is general. Other voltage-

dependencies could be realized through suitable material tailoring, by using composites, and by sectioning the transmission line layout. These alterations would afford relative assessments of voltage wave propagation in nonlinear transmission lines, and also provide for analyses of "shock wave" generation.

ACKNOWLEDGMENTS

I would like to thank Dr. Joshi for suggesting the topic of this thesis.

TABLE OF CONTENTS

Page

Section

1. INTRODUCTION 1
1.1 Aim 1
1.2 Background 2
1.3 Thesis Scope 2
1.4 Summary of Sections 3

2. WAVE PROPAGATION IN A NONLINEAR TRANSMISSION LINE 5
2.1 Derivation of Transmission Line Equations 5
2.2 Transmission Line Equations in Conservation Form 11
2.3 Shock Formation 16
2.4 Propagation Delay 21
2.5 Pre-Shock Rise Time Reduction 22
2.6 Fall Time Increase 23

3. NUMERICAL SCHEMES 25
3.1 Overview 25
3.2 Initial Condition Points 27
3.3 Left Boundary Points 28
3.4 Right Boundary Points 29
3.5 Interior Points 32

4. SIMULATION CONDITIONS AND IMPLEMENTATION DETAILS 48
4.1 Input Waveforms and Initial Conditions 48
4.2 Transmission Line Properties 51
4.3 Shock Formation Location 54
4.4 Numerical Scheme Implementation Details 55

5. RESULTS AND DISCUSSION 60
5.1 Step Input Simulations 60
5.2 Pulse Input Simulations 65
5.3 Pulse Generator 69

6. SUMMARIZING CONCLUSIONS AND FUTURE WORK 72
6.1 Summarizing Conclusions 72
6.2 Suggestions for Future Work 73

REFERENCES 75

VITA 77

LIST OF TABLES

Table Page

5-1. Expected and simulated propagation times for step waveform 62

5-2. Expected and simulated output rise times for step waveform 62

5-3. Expected and simulated propagation times for pulse waveform 66

5-4. Expected and simulated output rise times for pulse waveform 67

5-5. Expected and simulated output fall times for pulse waveform.....67

5-6. Maximum amplitudes and FDHMs of differentiated output waveforms.....70

LIST OF FIGURES

Figure Page

2-1. Circuit model for an infinitesimal, internal element of a transmission line 5

2-2. Circuit model for an infinitesimal, terminal element of a transmission line 8

2-3. Sample C versus V curve 17

2-4. Sample transmission line input voltage 17

2-5. Position of input voltages at time t 19

2-6. Position of input voltages at time t' 19

2-7. Sample input pulse waveform 23

3-1. Uniform space-time mesh.....26

4-1. Input step waveform 49

4-2. Input pulse waveform 50

4-3. A plot of charge per unit length versus voltage.....53

4-4. A plot of capacitance per unit length versus voltage.....54

5-1. LW scheme at 5m 63

5-2. Hybrid scheme at 5m.....63

5-3. LW scheme at 8m 63

5-4. Hybrid scheme at 8m.....63

5-5. LW scheme at 10m 63

5-6. Hybrid scheme at 10m.....63

5-7. LW scheme at 10.5m 64

5-8. Hybrid scheme at 10.5m.....64

5-9. LW scheme at 11m 64

Figure Page

5-10. Hybrid scheme at 11m 64

5-11. LW scheme at 12m 65

5-12. Hybrid scheme at 12m 65

5-13. Hybrid scheme at 15m 65

5-14. Hybrid scheme at 20m 65

5-15. LW scheme at 10m 67

5-16. Hybrid scheme at 10m 67

5-17. LW scheme at 10.5m 68

5-18. Hybrid scheme at 10.5m 68

5-19. LW scheme at 11m 68

5-20. Hybrid scheme at 11m 68

5-21. Hybrid scheme at 15m 68

5-22. Hybrid output at 5m 70

5-23. Differentiated hybrid output at 5m 70

5-24. Hybrid output at 10m 70

5-25. Differentiated hybrid output at 10m 70

5-26. Hybrid output at 12m 71

5-27. Differentiated hybrid output at 12m 71

5-28. Hybrid output at 15m 71

5-29. Differentiated hybrid output at 15m 71

SECTION 1

INTRODUCTION

1.1 Aim

The aim of this thesis is to understand wave propagation along a transmission line having a voltage-dependent capacitance. Such a transmission line is said to be nonlinear. The telegrapher's equations are the partial differential equations governing wave propagation along a transmission line. Since the telegrapher's equations are nonlinear for a nonlinear transmission line, they cannot be solved analytically; and thus the use of numerical schemes is required to find approximate solutions. The development of discontinuities, called shock waves, in the solution to the nonlinear telegrapher's equations makes their numerical solution nontrivial. In fact, this is an active area of research in applied mathematics [1]. To numerically simulate wave propagation along a transmission line having a voltage-dependent capacitance, this thesis presents and utilizes several schemes for finding approximate solutions to the nonlinear telegrapher's equations. The simulation results are compared to theoretical expectations. Finally, simulation results are used to briefly investigate the application of a nonlinear transmission line as a pulse generator for high voltage applications.

References follow the *IEEE Journal of Solid-State Circuits* format.

1.2 Background

Salinger [2] published the first work on nonlinear transmission lines in 1923. Riley [3] investigated wave propagation in a transmission line having a voltage-dependent capacitance using the method of characteristics, which is useful prior to shock formation. He also presented some theoretical properties of the shock waves that develop in such transmission lines. Alday [4] studied the application of a nonlinear transmission line as a pulse generator.

Courant and Friedrichs [5] provide a classic theoretical treatment of nonlinear hyperbolic systems of balance laws motivated by their investigation of gas dynamics. Dafermos [6] provides a modern theoretical treatment of nonlinear hyperbolic systems of balance laws from the more general perspective of continuum physics. Bloom [7] applies the theory of nonlinear hyperbolic systems of balance laws to investigate the nonlinear telegrapher's equations from an extremely theoretical perspective. Leveque [1] and Holden and Risebro [8] present numerical techniques to obtain approximate solutions to nonlinear hyperbolic systems of balance laws.

1.3 Thesis Scope

Mathematical treatments of nonlinear wave propagation have been discussed and studied in the literature. This is an important and active subject of study, and a large body of research has been reported in the archival literature. In this thesis, the goals are relatively modest. A mathematical analysis for voltage wave propagation in nonlinear

transmission lines is developed and applied to one particular case. Numerical approximations become necessary since analytical solutions do not exist. Thus, the primary objective is to understand and develop numerical schemes for analyses and demonstrate their successful implementation. In the process, the basic capability for modeling and simulation in this area of nonlinear voltage wave propagation will be demonstrated. Subsequently, other aspects such as more complicated nonlinear transmission line structures could be studied as the research scope expands in the future.

1.4 Summary of Sections

Section 2 derives the telegrapher's equations that model wave propagation along a transmission line having a voltage-dependent capacitance. This section goes on to show that these equations represent a nonlinear hyperbolic system of balance laws. Moreover, formulas predicting the expected behavior of solutions to these equations are presented.

Section 3 derives and analyzes three numerical schemes for obtaining approximate solutions to nonlinear hyperbolic systems of balance laws. In addition, it applies these schemes specifically to the nonlinear telegrapher's equations.

Section 5 summarizes the results of solving the nonlinear telegrapher's equations for several lengths of transmission line using the schemes presented in Section 3 subject to the parameters, initial conditions, and boundary conditions detailed in Section 4. Plots and tables supplement a comparison of the results to the theoretical expectations anticipated by the formulas presented in Section 2. Section 5 ends by using simulation results to investigate the application of a nonlinear transmission line as a pulse generator.

The final section, Section 6, summarizes the work presented in this thesis and suggests avenues for future investigations of nonlinear transmission lines.

SECTION 2

WAVE PROPAGATION IN A NONLINEAR TRANSMISSION LINE

In this section, several aspects of wave propagation in a nonlinear transmission line are examined. First, the wave equations governing the current and voltage in a transmission line are derived. Next, these equations are transformed into conservation form, a guise that commonly describes physical laws and that is readily amenable to solution via numerical methods. Then formulas predicting shock formation, propagation delay, rise time reduction, and fall time increase of a voltage waveform propagating in a lossless nonlinear transmission line are presented.

2.1 Derivation of Transmission Line Equations

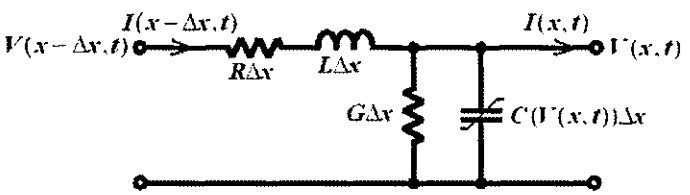

Figure 2-1. Circuit model for an infinitesimal, internal element of a transmission line.

This section derives the partial differential equations (PDEs) governing the current and voltage developed on a finite-length transmission line when subjected to an input voltage. The derivation here is similar to that presented by Johansson and Lundgren [9]. Consider a transmission line of length l terminated with a load resistance R_L. Such a line may be represented by a series of infinitesimal distributed elements. A circuit model

for an infinitesimal, internal element of length Δx is depicted in Figure 2-1. Here R, L, G, and C are the resistance, inductance, conductance, and capacitance per unit length, respectively. If $R = G = 0$, then the transmission line is said to be lossless; otherwise, the transmission line is lossy [10]. C is a function of the voltage V and is defined as $C(V) \equiv \frac{dq(V)}{dV}$, where q is charge per unit length. We assume that q and its derivative, C, are known functions of V. If C is non-constant (i.e. q is nonlinear), then the transmission line is said to be nonlinear; otherwise, the transmission line is linear.

$I(x-\Delta x,t)$, $V(x-\Delta x,t)$ are the current and voltage at position $x-\Delta x$ and time t; $I(x,t)$, $V(x,t)$ are the current and voltage at position x and time t. Let $\mathbb{R}$ denote the set of real numbers. We assume that $V:[0,l]\times(0,\infty)\to\mathbb{R}$ and $I:[0,l]\times(0,\infty)\to\mathbb{R}$ are C^1; this means that the partial derivatives $\frac{\partial V}{\partial x}$, $\frac{\partial V}{\partial t}$, $\frac{\partial I}{\partial x}$, and $\frac{\partial I}{\partial t}$ exist and are continuous [11].

By applying Kirchhoff's Voltage Law to the circuit model in Figure 2-1, we obtain:

$$V(x-\Delta x,t) - L\Delta x\frac{\partial I(x-\Delta x,t)}{\partial t} - R\Delta x I(x-\Delta x,t) - V(x,t) = 0. \tag{2-1}$$

Rearranging the above equation, we obtain:

$$\frac{V(x,t)-V(x-\Delta x,t)}{\Delta x} = -L\frac{\partial I(x-\Delta x,t)}{\partial t} - RI(x-\Delta x,t). \tag{2-2}$$

Now taking the limit as Δx approaches zero on both sides of this equation, we obtain:

$$\lim_{\Delta x \to 0} \frac{V(x,t) - V(x-\Delta x,t)}{\Delta x} = \lim_{\Delta x \to 0} [-L \frac{\partial I(x-\Delta x,t)}{\partial t} - RI(x-\Delta x,t)]. \tag{2-3}$$

Thus,

$$\frac{\partial V(x,t)}{\partial x} = -L \frac{\partial I(x,t)}{\partial t} - RI(x,t). \tag{2-4}$$

This may be written more succinctly as:

$$V_x(x,t) + LI_t(x,t) = -RI(x,t). \tag{2-5}$$

Applying Kirchhoff's Current Law (KCL) to the upper node of the circuit model in Figure 2-1, we obtain:

$$I(x-\Delta x,t) - I(x,t) - G\Delta x V(x,t) - C(V(x,t))\Delta x \frac{\partial V(x,t)}{\partial t} = 0. \tag{2-6}$$

Rearranging the above equation yields:

$$\frac{I(x,t) - I(x-\Delta x,t)}{\Delta x} = -GV(x,t) - C(V(x,t)) \frac{\partial V(x,t)}{\partial t}. \tag{2-7}$$

Taking the limit as Δx approaches zero on both sides of this equation gives:

$$\lim_{\Delta x \to 0} \frac{I(x,t) - I(x-\Delta x,t)}{\Delta x} = \lim_{\Delta x \to 0}[-GV(x,t) - C(V(x,t))\frac{\partial V(x,t)}{\partial t}]. \tag{2-8}$$

Therefore,

$$\frac{\partial I(x,t)}{\partial x} = -GV(x,t) - C(V(x,t))\frac{\partial V(x,t)}{\partial t}. \tag{2-9}$$

This may be written more succinctly as:

$$I_x(x,t) + C(V(x,t))V_t(x,t) = -GV(x,t). \tag{2-10}$$

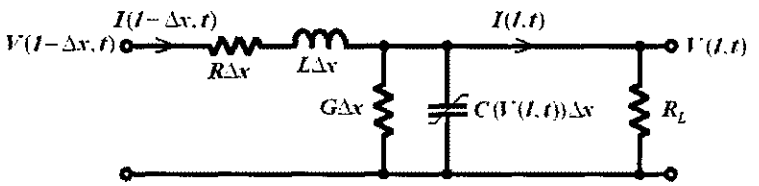

Figure 2-2. Circuit model for an infinitesimal, terminal element of a transmission line.

Figure 2-2 depicts an infinitesimal, terminal element of a transmission line of length Δx. Applying Kirchhoff's Voltage Law to the circuit model in Figure 2-2, we obtain:

$$V(l-\Delta x,t) - L\Delta x\frac{\partial I(l-\Delta x,t)}{\partial t} - R\Delta x I(l-\Delta x,t) - V(l,t) = 0. \tag{2-11}$$

Rearranging this equation gives:

$$\frac{V(l,t)-V(l-\Delta x,t)}{\Delta x}=-L\frac{\partial I(l-\Delta x,t)}{\partial t}-RI(l-\Delta x,t). \tag{2-12}$$

Taking the limit as Δx approaches zero on both sides of this equation, we obtain:

$$\lim_{\Delta x\to 0}\frac{V(l,t)-V(l-\Delta x,t)}{\Delta x}=\lim_{\Delta x\to 0}[-L\frac{\partial I(l-\Delta x,t)}{\partial t}-RI(l-\Delta x,t)]. \tag{2-13}$$

Thus,

$$\frac{\partial V(l,t)}{\partial x}=-L\frac{\partial I(l,t)}{\partial t}-RI(l,t). \tag{2-14}$$

Since $I(l,t)=\frac{V(l,t)}{R_L}$, $\frac{\partial I(l,t)}{\partial t}=\frac{1}{R_L}\frac{\partial V(l,t)}{\partial t}$. Substituting these equalities into (2-14), gives:

$$\frac{\partial V(l,t)}{\partial x}=-\frac{L}{R_L}\frac{\partial V(l,t)}{\partial t}-\frac{R}{R_L}V(l,t). \tag{2-15}$$

Equation (2-15) may be written more succinctly as:

$$V_x(l,t)+\frac{L}{R_L}V_t(l,t)=-\frac{R}{R_L}V(l,t). \tag{2-16}$$

Thus, the transmission line current, I, and voltage, V, must satisfy the following pair of inhomogeneous quasilinear partial differential equations:

$$\begin{cases} V_x(x,t)+LI_t(x,t)=-RI(x,t), \\ I_x(x,t)+C(V(x,t))V_t(x,t)=-GV(x,t), \end{cases} \qquad (x,t)\in(0,l)\times(0,\infty), \tag{2-17}$$

subject to the left and right boundary conditions:

$$\begin{cases} V(0,t)=f(t), \\ I(l,t)=\dfrac{V(l,t)}{R_L}, \\ V_x(l,t)+\dfrac{L}{R_L}V_t(l,t)=-\dfrac{R}{R_L}V(l,t), \end{cases} \qquad t\in(0,\infty), \tag{2-18}$$

and the initial conditions:

$$\begin{cases} I(x,0)=g(x), \\ V(x,0)=h(x), \end{cases} \qquad x\in(0,l). \tag{2-19}$$

2.2 Transmission Line Equations in Conservation Form

In this section, the partial differential equation problem prescribed by (2-17) through (2-19) is transformed to conservation form following Bloom [7]. We assume that the charge per unit length, q, as a function of voltage, V, is one-to-one and C^1; this means that $q(V_1) = q(V_2)$ only when $V_1 = V_2$ and that q' exists and is continuous. By the inverse function theorem [11], q possesses a C^1 inverse, v, such that:

$$v'(Q) = \frac{1}{q'(v(Q))}. \tag{2-20}$$

Since $C \equiv q'$,

$$v'(Q) = \frac{1}{C(v(Q))}. \tag{2-21}$$

As in the previous section, the voltage at (x,t) is $V(x,t)$. The charge per unit length at (x,t) is $Q(x,t)$. Thus, $V(x,t) = v(Q(x,t))$ and $Q(x,t) = q(V(x,t))$.

Since $V(x,t) = v(Q(x,t))$ implies that $V_x(x,t) = v'(Q(x,t))Q_x(x,t)$, the first equation of (2-17) becomes:

$$I_t(x,t) + \frac{v'(Q(x,t))}{L} Q_x(x,t) = -\frac{R}{L} I(x,t). \tag{2-22}$$

The second equation of (2-17) becomes:

$$Q_t(x,t)+I_x(x,t)=-Gv(Q(x,t)), \tag{2-23}$$

since $V_t(x,t)=v'(Q(x,t))Q_t(x,t)=\dfrac{Q_t(x,t)}{C(v(Q(x,t)))}=\dfrac{Q_t(x,t)}{C(V(x,t))}$.

In terms of Q, the left boundary condition of (2-18) is equivalent to:

$$Q(0,t)=q(V(0,t))=q(f(t))=\tilde{f}(t). \tag{2-24}$$

The right boundary conditions of (2-18) are equivalent to:

$$\begin{cases} I(l,t)=\dfrac{v(Q(l,t))}{R_L}, \\ v'(Q(l,t))Q_x(l,t)+\dfrac{L}{R_L}v'(Q(l,t))Q_t(l,t)=-\dfrac{R}{R_L}v(Q(l,t)), \end{cases} \tag{2-25}$$

Thus, the right boundary conditions of (2-18) are equivalent to:

$$\begin{cases} I(l,t)=\dfrac{v(Q(l,t))}{R_L}, \\ Q_x(l,t)+\dfrac{L}{R_L}Q_t(l,t)=-\dfrac{R}{R_L}\dfrac{v(Q(l,t))}{v'(Q(l,t))}, \end{cases} \tag{2-26}$$

In terms of Q, the initial voltage condition of (2-19) is equivalent to:

$$Q(x,0) = q(V(x,0)) = q(h(x)) = \tilde{h}(x). \tag{2-27}$$

Thus, the transmission line current, I, and charge per unit length, Q, must satisfy the following pair of inhomogeneous quasilinear partial differential equations:

$$\begin{cases} I_t(x,t) + \dfrac{v'(Q(x,t))}{L} Q_x(x,t) = -\dfrac{R}{L} I(x,t), \\ Q_t(x,t) + I_x(x,t) = -Gv(Q(x,t)), \end{cases} \qquad (x,t) \in (0,l) \times (0,\infty), \tag{2-28}$$

subject to the left and right boundary conditions:

$$\begin{cases} Q(0,t) = \tilde{f}(t), \\ I(l,t) = \dfrac{v(Q(l,t))}{R_L}, \\ Q_x(l,t) + \dfrac{L}{R_L} Q_t(l,t) = -\dfrac{R}{R_L} \dfrac{v(Q(l,t))}{v'(Q(l,t))}, \end{cases} \qquad t \in (0,\infty), \tag{2-29}$$

and the initial conditions:

$$\begin{cases} I(x,0) = g(x) = \tilde{g}(x), \\ Q(x,0) = \tilde{h}(x), \end{cases} \qquad x \in (0,l). \tag{2-30}$$

Using the following definitions:

$$\mathbf{u} = \begin{pmatrix} I \\ Q \end{pmatrix}, \tag{2-31}$$

$$\mathbf{f}(\mathbf{u}) = \begin{pmatrix} \dfrac{v(Q)}{L} \\ I \end{pmatrix}, \tag{2-32}$$

$$\mathbf{A}(\mathbf{u}) = \mathbf{f}'(\mathbf{u}) = \begin{pmatrix} 0 & \dfrac{v'(Q)}{L} \\ 1 & 0 \end{pmatrix}, \tag{2-33}$$

$$\mathbf{b}(\mathbf{u}) = \begin{pmatrix} \dfrac{-R}{L} I \\ -Gv(Q) \end{pmatrix}, \tag{2-34}$$

the system of PDEs (2-28) may be rewritten succinctly in either form below:

$$\mathbf{u}_t + \mathbf{f}(\mathbf{u})_x = \mathbf{b}(\mathbf{u}), \tag{2-35}$$

$$\mathbf{u}_t + \mathbf{A}(\mathbf{u})\mathbf{u}_x = \mathbf{b}(\mathbf{u}). \tag{2-36}$$

A system of PDEs cast in the form of (2-35) or (2-36) represents a first-order system of quasilinear partial differential equations in two independent variables [12]. If $\mathbf{b} \neq 0$ (i.e. $R \neq 0$ or $G \neq 0$), the system is inhomogeneous (nonhomogeneous) [12]; therefore, a lossy transmission line is modeled by an inhomogeneous system of PDEs. If $\mathbf{b} \equiv 0$ (i.e. $R = G = 0$), then the system is homogeneous [12]; that is, a lossless transmission line is modeled by a homogeneous system of PDEs. If $\mathbf{A}(\mathbf{u})$ is constant (i.e. $\mathbf{A}(\mathbf{u})$ is not a function of $\mathbf{u}$), the system is linear; otherwise, the system is nonlinear. For the system (2-

28) representing the transmission line, note that $\mathbf{A}(\mathbf{u})$ is constant if and only if $v'(Q)$ is constant. Recall that a transmission line is linear if and only if $C(V)$ is constant. Therefore, by (2-21), the system of PDEs (2-28) is linear if and only if the transmission line is linear. A system of PDEs in the form of (2-35) or (2-36) is called a system of conservation laws [12]. When the system is inhomogeneous (i.e. $\mathbf{b} \neq 0$), it is often called a system of balance laws instead of a system of conservation laws [1].

The eigenvalues of $\mathbf{A}(\mathbf{u})$ are the two roots of $|\mathbf{A}(\mathbf{u}) - \lambda\mathbf{I}|$, where $\mathbf{I}$ is the 2x2 identity matrix. Since:

$$|\mathbf{A}(\mathbf{u}) - \lambda\mathbf{I}| = \begin{vmatrix} -\lambda & \dfrac{v'(Q)}{L} \\ 1 & -\lambda \end{vmatrix} = \lambda^2 - \frac{v'(Q)}{L}, \tag{2-37}$$

the roots of $|\mathbf{A}(\mathbf{u}) - \lambda\mathbf{I}|$ are:

$$\lambda = \pm\sqrt{\frac{v'(Q)}{L}}. \tag{2-38}$$

If $v'(Q) > 0$ for all Q, then the eigenvalues of $\mathbf{A}(\mathbf{u})$ are real and distinct. A system of PDEs in the form of (2-35) or (2-36) such that the eigenvalues of $\mathbf{A}(\mathbf{u})$ are real and distinct is called strictly hyperbolic [12]. Hence, the system of PDEs representing the transmission line is strictly hyperbolic provided that $v'(Q) > 0$ for all Q.

If $v'(Q) > 0$ for all Q, $v'(Q)$ is nonconstant, and $\mathbf{b} \neq 0$, then the transmission line equations ((2-35) or (2-36)) describe a 2x2, inhomogeneous, nonlinear, strictly hyperbolic system of conservation laws. Equivalently, if $v'(Q) > 0$ for all Q, $v'(Q)$ is nonconstant, and $\mathbf{b} \neq 0$, then the transmission line equations ((2-35) or (2-36)) describe a 2x2, nonlinear, strictly hyperbolic system of balance laws.

2.3 Shock Formation

The explanations and equations presented in this section were inspired by Jones [13]. Recall that a voltage pulse of amplitude A propagates along a lossless transmission line with speed:

$$\gamma = \frac{1}{\sqrt{LC(A)}}. \tag{2-39}$$

(2-39) specifies an inverse relationship between propagation speed and capacitance per unit length. To understand the implication of this inverse relationship, consider a possible C versus V curve such as that given in Figure 2-3 (see Section 5.1). Since C is non-constant, a transmission line constructed from a dielectric with this C versus V characteristic is nonlinear. For this particular curve, high magnitude voltages yield small capacitances per unit length; in contrast, low magnitude voltages yield large capacitances per unit length. Thus by (2-39), the higher magnitude voltages travel faster than lower magnitude voltages.

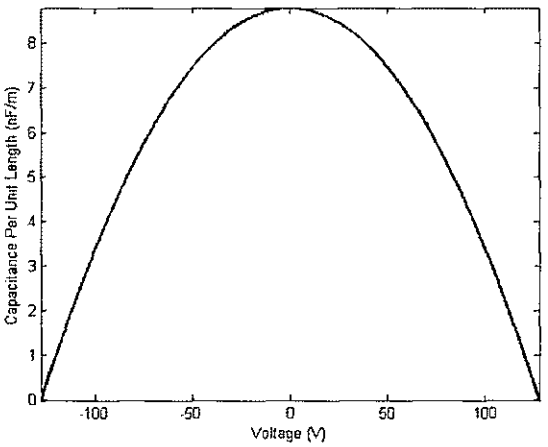

Figure 2-3. Sample C versus V curve.

Consider the voltage waveform of Figure 2-4 injected into the input end of the nonlinear transmission line. The higher amplitude voltages propagate faster than the lower amplitude voltages. The higher amplitude, faster-moving voltages will be expected to "catch up" to the lower amplitude, slower-moving voltages since the higher voltages enter the transmission line later than the lower voltages.

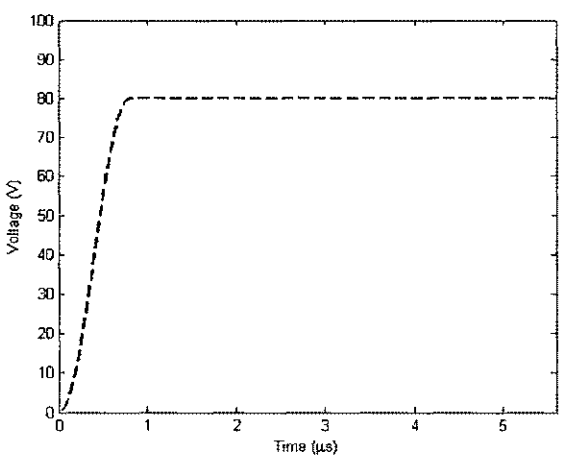

Figure 2-4. Sample transmission line input voltage.

Eventually, the higher amplitude, faster-moving voltages will be expected to overtake the lower amplitude, slower-moving voltages. Thus, one might expect the voltage in the transmission line to become multi-valued at the crossings. A multi-valued voltage in a transmission line is physically impossible. Instead, a discontinuity develops where the higher amplitude, faster-moving voltages begin to overtake the lower amplitude, slower-moving voltages. The "shock wave" is the locus of points in $[0,l]\times[0,\infty)$ where the voltage is discontinuous [7].

To determine where and when shock wave formation occurs in a lossless, nonlinear transmission line, let $f(s)=V(0,s)$ represent the voltage injected into the transmission line at time s. Then for $t \geq s$, the position at time t of the voltage injected into the transmission line at time s is:

$$x(t,s)=\frac{t-s}{\sqrt{LC(f(s))}}. \tag{2-40}$$

Note that (2-40) only holds prior to shock formation. Before shock formation occurs, at a fixed time t, $x(t,0) \geq x(t,s_1) > x(t,s_2) \geq x(t,t)=0$ for $0 \leq s_1 < s_2 \leq t$; that is, x decreases monotonically as a function of s for a fixed t. Thus the positions of the input voltages at time t might look like the plot in Figure 2-5 below.

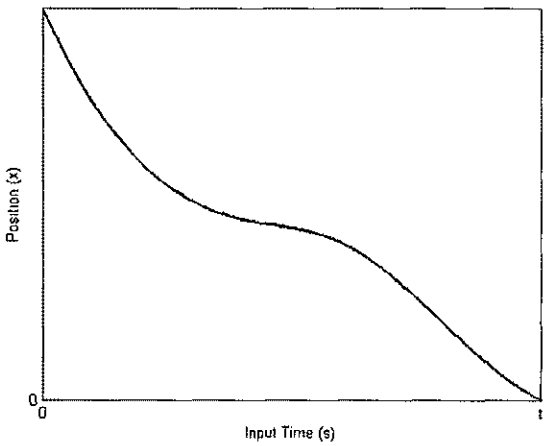

Figure 2-5. Position of input voltages at time t.

At a slightly later time, t', the positions of the input voltages might look like Figure 2-6 below. For distinct input times, $s_1 < s_2$, voltage overtaking occurs at time t' if $x(s_1,t') = x(s_2,t')$. Thus, observe that voltage overtaking occurs at the critical point in Figure 2-6. Recall that a critical point of a function is a point in its domain where the function's derivative evaluates to zero [11].

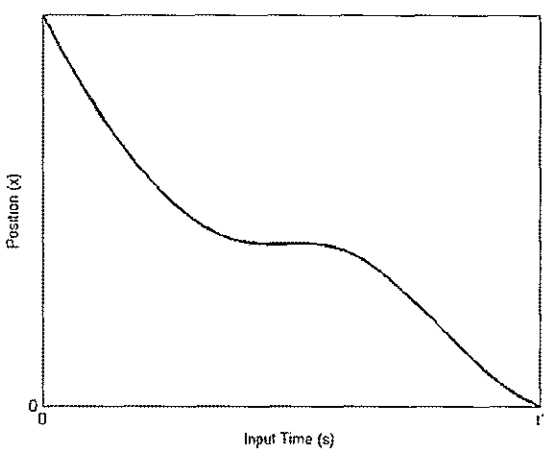

Figure 2-6. Position of input voltages at time t'. Voltage overtaking occurs at the critical point.

Thus, shock formation occurs at the earliest time $t > 0$ such that the graph of $x(t,s)$ $(t \geq s \geq 0)$ contains a critical point. That is, shock formation occurs at the minimum time t such that:

$$\frac{\partial x(t,s)}{\partial s} = 0. \tag{2-41}$$

Calculating the partial derivative in (2-41) using (2-40) yields:

$$\frac{\partial x(t,s)}{\partial s} = \frac{-\sqrt{LC(f(s))} - (t-s)\dfrac{LC'(f(s))f'(s)}{2\sqrt{LC(f(s))}}}{LC(f(s))} = 0 \Leftrightarrow \tag{2-42}$$

$$(t-s)\frac{LC'(f(s))f'(s)}{2\sqrt{LC(f(s))}} = -\sqrt{LC(f(s))} \Leftrightarrow \tag{2-43}$$

$$(t-s)LC'(f(s))f'(s) = -2LC(f(s)) \Leftrightarrow \tag{2-44}$$

$$t = \theta(s) = s - \frac{2C(f(s))}{C'(f(s))f'(s)}. \tag{2-45}$$

Observe from (2-45) that since $t \geq s \geq 0$, shock formation does not occur if $C'(f(s))f'(s) > 0$ for all s. Also note that the time at which shock formation occurs depends on the shapes of C and of f; the time of shock formation does not depend on L. To determine when shock formation occurs, we determine the minimum of θ:

$$\theta'(s) = 1 - \frac{C'(f(s))f'(s)2C'(f(s))f'(s) - 2C(f(s))[C''(f(s))(f'(s))^2 + C'(f(s))f''(s)]}{[C'(f(s))f'(s)]^2} = 0 \Leftrightarrow \quad (2\text{-}46)$$

$$1 - 2 + \frac{2C(f(s))[C''(f(s))(f'(s))^2 + C'(f(s))f''(s)]}{[C'(f(s))f'(s)]^2} = 0 \Leftrightarrow \quad (2\text{-}47)$$

$$[C'(f(s))f'(s)]^2 = 2C(f(s))[C''(f(s))(f'(s))^2 + C'(f(s))f''(s)]. \quad (2\text{-}48)$$

The implicit equation given by (2-48) may be solved to determine the input time $\bar{s}$ that minimizes θ. Therefore, shock formation occurs at time $\bar{t} = \theta(\bar{s})$. Since $\frac{\partial x(\bar{t}, \bar{s})}{\partial s} = 0$, shock formation occurs at position $\bar{x} = x(\bar{t}, \bar{s}) = \frac{\bar{t} - \bar{s}}{\sqrt{LC(f(\bar{s}))}}$. For the remainder of this thesis, $\bar{x}$ shall denote the position at which shock formation occurs in a lossless nonlinear transmission line.

2.4 Propagation Delay

Consider a lossless nonlinear transmission line of length l. Assume that the transmission line is initially at rest (i.e. the current and voltage at all points on the line are zero at time zero). Suppose that a voltage waveform f is injected into the transmission line. Then the voltage that enters the transmission line at time s is $f(s)$. Suppose that $f(s)$ is not overtaken by faster moving voltages at it propagates along the length of transmission line. In light of (2-39), $f(s)$ reaches the terminal end at time t, given by:

$$t = s + l\sqrt{LC(f(s))}. \quad (2\text{-}49)$$

2.5 Pre-Shock Rise Time Reduction

In this section we consider a lossless nonlinear transmission line of length $l < \bar{x}$, where $\bar{x}$ denotes the shock formation position given in Section 2.3. We assume that the transmission line is initially at rest (i.e. the current and voltage at all points on the line are zero at time zero). Consider a rising edge input waveform f with final amplitude A, like the one depicted in Figure 2-4. Throughout this thesis, the rise time of a rising edge is defined as the time for the waveform to increase from 0.1 to 0.9 of its final value [14]. Let s_1 denote the input time at which $f(s_1) = 0.1A$, and let $s_2 > s_1$ denote the later input time at which $f(s_2) = 0.9A$. That is, the rise time of the input waveform is $s_2 - s_1$. In light of (2-49), the voltage that enters the transmission line at time s_1 reaches the terminal end at time t_1, given by:

$$t_1 = s_1 + l\sqrt{LC(f(s_1))} = s_1 + l\sqrt{LC(0.1A)}, \tag{2-50}$$

and the voltage that enters the transmission line at time s_2 reaches the terminal end at time t_2, given by:

$$t_2 = s_2 + l\sqrt{LC(f(s_2))} = s_2 + l\sqrt{LC(0.9A)}. \tag{2-51}$$

Hence, the rise time of the output waveform is:

$$t_2 - t_1 = (s_2 - s_1) + l\sqrt{L}(\sqrt{C(0.9A)} - \sqrt{C(0.1A)}). \tag{2-52}$$

If one assumes that C decreases monotonically for positive voltages V (such as occurs in Figure 2-3), then $\sqrt{C(0.9A)} - \sqrt{C(0.1A)} < 0$ and the rise time of the output waveform is less than that of the input waveform. Moreover, the output rise time decreases as l increases.

2.6 Fall Time Increase

In this section we consider a lossless nonlinear transmission line of length l. We assume that the transmission line is initially at rest (i.e. the current and voltage at all points on the line are zero at time zero). Consider an input pulse f with amplitude A, like the one depicted in Figure 2-7.

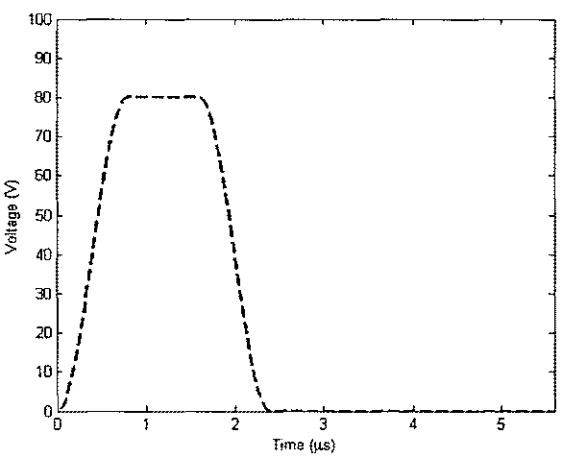

Figure 2-7. Sample input pulse waveform.

Throughout this thesis, the fall time of a falling edge is defined as the time for the waveform to decrease from 0.9 to 0.1 of its maximum value. Let s_1 denote the input time at which $f(s_1) = 0.9A$, and let $s_2 > s_1$ denote the later input time at which $f(s_2) = 0.1A$. That is, the fall time of the input waveform is $s_2 - s_1$. In light of (2-49), the voltage that enters the transmission line at time s_1 reaches the terminal end at time t_1, given by:

$$t_1 = s_1 + l\sqrt{LC(f(s_1))} = s_1 + l\sqrt{LC(0.9A)}, \tag{2-53}$$

and the voltage that enters the transmission line at time s_2 reaches the terminal end at time t_2, given by:

$$t_2 = s_2 + l\sqrt{LC(f(s_2))} = s_2 + l\sqrt{LC(0.1A)}. \tag{2-54}$$

Hence, the rise time of the output waveform is:

$$t_2 - t_1 = (s_2 - s_1) + l\sqrt{L}(\sqrt{C(0.1A)} - \sqrt{C(0.9A)}). \tag{2-55}$$

If one assumes that C decreases monotonically for positive voltages V (such as occurs in Figure 2-3), then $\sqrt{C(0.1A)} - \sqrt{C(0.9A)} > 0$ and the fall time of the output waveform exceeds that of the input waveform. Moreover, the output fall time increases as l increases.

SECTION 3

NUMERICAL SCHEMES

This section presents the numerical schemes employed to obtain approximate solutions to the PDE problem defined by (2-28)-(2-30).

3.1 Overview

To solve (2-28)-(2-30) over the time interval $[0,T]$, we define a uniform mesh of discrete points in space and time determined by a distance step δ and a time step ε:

$$\Gamma = \{(x_k, t^n) = (k\delta, n\varepsilon) : k = 0,1,2,...,K-1 \quad \text{and} \quad n = 0,1,2,...,N-1\}, \tag{3-1}$$

where $(K-1)\delta = l$ and $(N-1)\varepsilon = T$. Figure 3-1 depicts such a mesh. Let $\lambda \equiv \frac{\varepsilon}{\delta}$ denote the ratio of the time step to the distance step. We assume throughout that this ratio is fixed. Thus, if Γ is modified to another mesh Γ' by choosing a new time step ε', then the distance step of Γ' must be $\delta' = \frac{\varepsilon'}{\lambda}$.

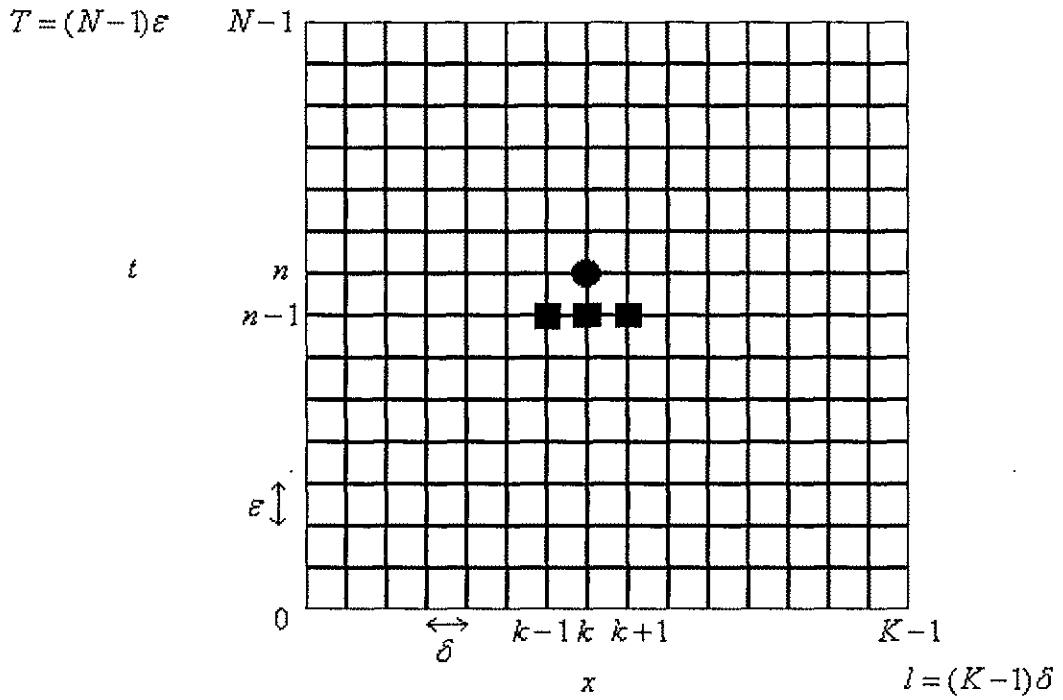

Figure 3-1. Uniform space-time mesh.

Let $\mathbf{u}(x,t)=\begin{pmatrix} I(x,t) \\ Q(x,t) \end{pmatrix}$ denote the true solution to (2-28)-(2-30) at $(x,t)\in[0,l]\times[0,T]$. This section presents numerical formulae for approximating $\mathbf{u}(x_k,t^n)=\mathbf{u}(k\delta,n\varepsilon)$, where $k=0,1,2,...,K-1$ and $n=0,1,2,...,N-1$. We let

$$\mathbf{u}_k^n=\begin{pmatrix} I_k^n \\ Q_k^n \end{pmatrix} \tag{3-2}$$

denote the approximation to the true value of $\mathbf{u}$ at (x_k,t^n), $\mathbf{u}(x_k,t^n)$. For $k=0,1,2,...,K-1$, $\mathbf{u}_k^0$ is calculated exactly using the initial conditions (2-30) (see Section 3.2). Next, (2-28) and (2-29) are used to calculate $\mathbf{u}_k^n$ for $k=0,1,2,...,K-1$ and

$n=1,2,...,N-1$. For $n=1,2,...,N-1$, $\mathbf{u}_0^n$ is calculated immediately after $\mathbf{u}_{K-1}^{n-1}$ (see Section 3.3). For $k=1,2,...,K-1$ and $n=1,2,...,N-1$, $\mathbf{u}_k^n$ is calculated immediately after $\mathbf{u}_{k-1}^n$ (see Sections 3.4 and 3.5).

In general, $\mathbf{u}_k^n$ is a function of previously calculated approximations; that is, $\mathbf{u}_k^n = \mathrm{N}(\{\mathbf{u}_j^m\}_{j\neq k, m\neq n})$. If one assumes that $\mathbf{u}_j^m = \mathbf{u}(j\delta, m\varepsilon)$ for all $j\neq k$ and all $m\neq n$, then the local truncation error in the calculation of $\mathbf{u}_k^n$ is defined as [1]:

$$\boldsymbol{\tau}_k^n \equiv \frac{\mathbf{u}(k\delta,n\varepsilon)-\mathbf{u}_k^n}{\varepsilon} = \frac{\mathbf{u}(k\delta,n\varepsilon)-\mathrm{N}(\{\mathbf{u}(j\delta,m\varepsilon)\}_{j\neq k,m\neq n})}{\varepsilon}. \tag{3-3}$$

The approximation formula $\mathbf{u}_k^n = \mathrm{N}(\{\mathbf{u}_j^m\}_{j\neq k,m\neq n})$ is said to be accurate of order p if the local truncation error is $\boldsymbol{\tau}_k^n = O(\varepsilon^p)$ [1].

3.2 Initial Condition Points

For $k=0,1,2,...,K-1$, the initial conditions of (2-30) may be used to exactly determine $\mathbf{u}_k^0$:

$$\mathbf{u}_k^0 = \begin{pmatrix} \tilde{g}(k\delta) \\ \tilde{h}(k\delta) \end{pmatrix}. \tag{3-4}$$

Since $\mathbf{u}_k^0 = \mathbf{u}(k\delta,0)$, the local truncation error is 0 in the above calculation.

3.3 Left Boundary Points

For $n = 1, 2, ..., N-1$, the first equation of (2-29) may be used to exactly calculate Q_0^n:

$$Q_0^n = \tilde{f}(n\varepsilon). \tag{3-5}$$

Recall that the first equation of (2-28) is equivalent to the first equation of (2-17):

$$V_x(x,t) + LI_t(x,t) = -RI(x,t). \tag{3-6}$$

Substituting

$$I_t(0,t^{n-1}) = \frac{I(0,t^n) - I(0,t^{n-1})}{\varepsilon} + O(\varepsilon) \tag{3-7}$$

and

$$\begin{aligned} V_x(0,t^{n-1}) &= \frac{V(\delta,t^{n-1}) - V(0,t^{n-1})}{\delta} + O(\delta) \\ &= \frac{v(Q(\delta,t^{n-1})) - v(Q(0,t^{n-1}))}{\delta} + O(\delta) \end{aligned} \tag{3-8}$$

into (3-6) and solving for $I(0,t^n)$ yields:

$$I(0,t^n) = I(0,t^{n-1}) - \frac{\lambda}{L}(v(Q(\delta,t^{n-1})) - v(Q(0,t^{n-1}))) - \frac{\varepsilon R}{L} I(0,t^{n-1}) + O(\varepsilon^2) + O(\varepsilon\delta). \quad (3\text{-}9)$$

Thus for $n = 1,2,...,N-1$, $I(0,t^n)$ may be approximated to first-order accuracy by I_0^n:

$$I_0^n = (1 - \frac{\varepsilon R}{L}) I_0^{n-1} - \frac{\lambda}{L}(v(Q_1^{n-1}) - v(Q_0^{n-1})). \quad (3\text{-}10)$$

Combining (3-10) and (3-5) gives a first-order formula for approximating $\mathbf{u}(0,n\varepsilon)$ for $n = 1,2,...,N-1$:

$$\mathbf{u}_0^n = \begin{pmatrix} (1 - \frac{\varepsilon R}{L}) I_0^{n-1} - \frac{\lambda}{L}(v(Q_1^{n-1}) - v(Q_0^{n-1})) \\ \tilde{f}(n\varepsilon) \end{pmatrix}. \quad (3\text{-}11)$$

3.4 Right Boundary Points

Assume that $n = 1,2,...,N-1$. This section uses the right boundary conditions of (2-29) to derive formulae for calculating $\mathbf{u}_{K-1}^n$. Note that the third equation of (2-29) is equivalent to the third equation of (2-18):

$$V_x(l,t)+\frac{L}{R_L}V_t(l,t)=-\frac{R}{R_L}V(l,t). \tag{3-12}$$

Substituting

$$\begin{aligned} V_x(l,t^n) &= \frac{V(l,t^n)-V(l-\delta,t^n)}{\delta}+O(\delta) \\ &= \frac{v(Q(l,t^n))-v(Q(l-\delta,t^n))}{\delta}+O(\delta) \end{aligned} \tag{3-13}$$

and

$$\begin{aligned} V_t(l,t^n) &= \frac{V(l,t^n)-V(l,t^{n-1})}{\varepsilon}+O(\varepsilon) \\ &= \frac{v(Q(l,t^n))-v(Q(l,t^{n-1}))}{\varepsilon}+O(\varepsilon) \end{aligned} \tag{3-14}$$

into (3-12) and solving for $v(Q(l,t^n))$ gives:

$$v(Q(l,t^n))=\alpha v(Q(l-\delta,t^n))+\beta v(Q(l,t^{n-1}))+O(\zeta\delta)+O(\zeta\varepsilon), \tag{3-15}$$

where $\zeta=\left[\frac{R}{R_L}+\frac{1}{\delta}+\frac{L}{\varepsilon R_L}\right]^{-1}$, $\alpha=\frac{\zeta}{\delta}$, and $\beta=\frac{L\zeta}{R_L\varepsilon}$. By using a Taylor series approximation of $\varepsilon\frac{R}{R_L}+\left(\lambda+\frac{L}{R_L}\right)$ for small ε we obtain:

$$\begin{aligned}\zeta &= \left[\frac{R}{R_L}+\frac{1}{\delta}+\frac{L}{\varepsilon R_L}\right]^{-1} \\ &= \frac{\varepsilon}{\varepsilon\dfrac{R}{R_L}+\left(\lambda+\dfrac{L}{R_L}\right)} \\ &= \varepsilon\left(\left(\lambda+\frac{L}{R_L}\right)^{-1}+O(\varepsilon)\right) \\ &= O(\varepsilon).\end{aligned} \tag{3-16}$$

Thus, (3-15) may be rewritten:

$$v(Q(l,t^n)) = \alpha v(Q(l-\delta,t^n)) + \beta v(Q(l,t^{n-1})) + O(\varepsilon\delta) + O(\varepsilon^2). \tag{3-17}$$

Since q is smooth,

$$\begin{aligned}Q(l,t^n) &= q(\alpha v(Q(l-\delta,t^n)) + \beta v(Q(l,t^{n-1})) + O(\varepsilon\delta) + O(\varepsilon^2)) \\ &= q(\alpha v(Q(l-\delta,t^n)) + \beta v(Q(l,t^{n-1}))) + O(\varepsilon\delta) + O(\varepsilon^2).\end{aligned} \tag{3-18}$$

Therefore, a first-order approximation of $Q(l,t^n)$ is:

$$Q_{K-1}^n = q(\alpha v(Q_{K-2}^n) + \beta v(Q_{K-1}^{n-1})). \tag{3-19}$$

The second equation of (2-29),

$$I(l,t)=\frac{v(Q(l,t))}{R_L}, \tag{3-20}$$

suggests the following first-order approximation of $I((K-1)\delta,t^n)$:

$$I_{K-1}^n=\frac{\alpha v(Q_{K-2}^n)+\beta v(Q_{K-1}^{n-1})}{R_L}, \tag{3-21}$$

where (3-17) has been used to approximate $v(Q(l,t^n))$.

Combining (3-21) and (3-19) gives a first-order accurate formula for approximating $\mathbf{u}((K-1)\delta,n\varepsilon)$:

$$\mathbf{u}_{K-1}^n=\begin{pmatrix}\dfrac{\alpha v(Q_{K-2}^n)+\beta v(Q_{K-1}^{n-1})}{R_L}\\ q(\alpha v(Q_{K-2}^n)+\beta v(Q_{K-1}^{n-1}))\end{pmatrix}. \tag{3-22}$$

3.5 Interior Points

Assume that $k=1,2,...,K-2$ and $n=1,2,...,N-1$. This section presents three numerical schemes that exploit (2-28) to approximate $\mathbf{u}(x_k,t^n)$. The Lax-Friedrichs (LF) scheme [15] provides a first-order approximation, while the Lax-Wendroff (LW) scheme [15] offers a second-order approximation. The hybrid scheme [15] approximates $\mathbf{u}(x_k,t^n)$ via a weighted average of the LF and LW approximations.

The LF and LW schemes described by Lax [15] only apply to homogeneous systems (i.e. $\mathbf{b} \equiv 0$). The fractional-step and unsplit methods [1] are two techniques that adapt these schemes to solve inhomogeneous systems. The adapted schemes presented here follow the unsplit method [1].

3.5.1 Preliminaries

Before delving into the specifics of these approximation schemes, we use (2-28) to express the first and second temporal partial derivatives of $\mathbf{u}$ in terms of spatial partial derivatives. In conjunction with a Taylor series expansion in time at (x_k, t^{n-1}), the LF and LW schemes exploit these relations to calculate $\mathbf{u}_k^n$ in terms of $\mathbf{u}_{k-1}^{n-1}$, $\mathbf{u}_k^{n-1}$, and $\mathbf{u}_{k+1}^{n-1}$. Recall (2-28):

$$\begin{cases} I_t(x,t) + \dfrac{v'(Q(x,t))}{L} Q_x(x,t) = -\dfrac{R}{L} I(x,t), \\ Q_t(x,t) + I_x(x,t) = -Gv(Q(x,t)), \end{cases} \qquad (x,t) \in (0,l) \times (0,\infty). \tag{3-23}$$

Recalling the definitions given by (2-31)-(2-34), (3-23) may be written succinctly in the form:

$$\mathbf{u}_t + \mathbf{f}(\mathbf{u})_x = \mathbf{b}(\mathbf{u}). \tag{3-24}$$

Thus,

$$\mathbf{u}_t = -\mathbf{f}(\mathbf{u})_x + \mathbf{b}(\mathbf{u}). \tag{3-25}$$

By differentiating (3-25) with respect to time, we obtain:

$$\begin{aligned}
\mathbf{u}_{tt} &= -\mathbf{f}(\mathbf{u})_{xt} + \mathbf{b}(\mathbf{u})_t \\
&= -\mathbf{f}(\mathbf{u})_{tx} + \boldsymbol{\gamma}(\mathbf{u})\mathbf{u}_t \\
&= -(\mathbf{A}(\mathbf{u})\mathbf{u}_t)_x + \boldsymbol{\gamma}(\mathbf{u})(-\mathbf{f}(\mathbf{u})_x + \mathbf{b}(\mathbf{u})) \\
&= -(\mathbf{A}(\mathbf{u})(-\mathbf{f}(\mathbf{u})_x + \mathbf{b}(\mathbf{u})))_x + \boldsymbol{\gamma}(\mathbf{u})(-\mathbf{f}(\mathbf{u})_x + \mathbf{b}(\mathbf{u})) \\
&= (\mathbf{A}(\mathbf{u})\mathbf{f}(\mathbf{u})_x)_x - (\mathbf{A}(\mathbf{u})\mathbf{b}(\mathbf{u}))_x - \boldsymbol{\gamma}(\mathbf{u})\mathbf{f}(\mathbf{u})_x + \boldsymbol{\gamma}(\mathbf{u})\mathbf{b}(\mathbf{u}),
\end{aligned} \tag{3-26}$$

where

$$\boldsymbol{\gamma}(\mathbf{u}) = \mathbf{b}'(\mathbf{u}) = \begin{pmatrix} \dfrac{-R}{L} & 0 \\ 0 & -Gv'(Q) \end{pmatrix}. \tag{3-27}$$

When evaluated at (x_k, t^{n-1}), $\mathbf{f}(\mathbf{u})_x$ may be represented by the centered difference quotient:

$$\mathbf{f}(\mathbf{u})_x(x_k, t^{n-1}) = \frac{1}{2\delta}\{\mathbf{f}(\mathbf{u}(x_{k+1}, t^{n-1})) - \mathbf{f}(\mathbf{u}(x_{k-1}, t^{n-1}))\} + \frac{\delta^2}{6}\mathbf{f}(\mathbf{u})_{xxx}(x_k, t^{n-1}) + O(\delta^4). \tag{3-28}$$

Thus, evaluating (3-25) at (x_k, t^{n-1}) and making use of (3-28) gives:

$$\mathbf{u}_t(x_k,t^{n-1}) = \frac{-1}{2\delta}\{\mathbf{f}(\mathbf{u}(x_{k+1},t^{n-1})) - \mathbf{f}(\mathbf{u}(x_{k-1},t^{n-1}))\} + \mathbf{b}(\mathbf{u}(x_k,t^{n-1})) + \left[\frac{-\delta^2}{6}\mathbf{f}(\mathbf{u})_{xxx}(x_k,t^{n-1}) + O(\delta^4)\right]. \tag{3-29}$$

Before deriving an expression for $(\mathbf{A}(\mathbf{u})\mathbf{f}(\mathbf{u})_x)_x$, consider a smooth function g. Then Taylor's theorem provides the following relations:

$$g(x+\frac{\delta}{2}) = g(x) + \frac{\delta}{2}g'(x) + \frac{1}{2}\left(\frac{\delta}{2}\right)^2 g''(x) + O(\delta^3), \tag{3-30}$$

$$g(x+\frac{\delta}{2}) = g(x+\delta) - \frac{\delta}{2}g'(x+\delta) + \frac{1}{2}\left(\frac{\delta}{2}\right)^2 g''(x+\delta) + O(\delta^3), \tag{3-31}$$

$$g'(x+\delta) = g'(x) + \delta g''(x) + O(\delta^2), \tag{3-32}$$

and

$$g''(x+\delta) = g''(x) + O(\delta). \tag{3-33}$$

Halving the sum of (3-30) and (3-31) and then utilizing (3-32) and (3-33) gives:

$$g(x+\frac{\delta}{2}) = \frac{g(x+\delta)+g(x)}{2} + \frac{\delta}{4}(g'(x) - g'(x+\delta)) + \frac{\delta^2}{16}(g''(x) + g''(x+\delta)) + O(\delta^3)$$
$$= \frac{g(x+\delta)+g(x)}{2} + \frac{\delta}{4}(-\delta g''(x)) + \frac{\delta^2}{16}(2g''(x)) + O(\delta^3) \qquad (3\text{-}34)$$
$$= \frac{g(x+\delta)+g(x)}{2} - \frac{\delta^2}{8} g''(x) + O(\delta^3).$$

Replacing δ with $-\delta$ in (3-34) yields:

$$g(x-\frac{\delta}{2}) = \frac{g(x)+g(x-\delta)}{2} - \frac{\delta^2}{8} g''(x) + O(\delta^3). \qquad (3\text{-}35)$$

When evaluated at (x_k, t^{n-1}), $(\mathbf{A}(\mathbf{u})\mathbf{f}(\mathbf{u})_x)_x$ may be represented by using a succession of centered difference quotients in conjunction with (3-34) and (3-35):

$$
\begin{aligned}
(\mathbf{A}(\mathbf{u})\mathbf{f}(\mathbf{u})_x)_x(x_k,t^{n-1}) &= \frac{1}{\delta}\{\mathbf{A}(\mathbf{u}(x_k+\frac{\delta}{2},t^{n-1}))\mathbf{f}(\mathbf{u})_x(x_k+\frac{\delta}{2},t^{n-1}) \\
&\quad -\mathbf{A}(\mathbf{u}(x_k-\frac{\delta}{2},t^{n-1}))\mathbf{f}(\mathbf{u})_x(x_k-\frac{\delta}{2},t^{n-1})\}+O(\delta^2) \\
&= \frac{1}{\delta}\{\mathbf{A}(\mathbf{u}(x_k+\frac{\delta}{2},t^{n-1}))\left(\frac{\mathbf{f}(\mathbf{u}(x_{k+1},t^{n-1}))-\mathbf{f}(\mathbf{u}(x_k,t^{n-1}))}{\delta}-\frac{\delta^2}{24}\mathbf{f}(\mathbf{u})_{xxx}(x_k+\frac{\delta}{2},t^{n-1})+O(\delta^4)\right) \\
&\quad -\mathbf{A}(\mathbf{u}(x_k-\frac{\delta}{2},t^{n-1}))\left(\frac{\mathbf{f}(\mathbf{u}(x_k,t^{n-1}))-\mathbf{f}(\mathbf{u}(x_{k-1},t^{n-1}))}{\delta}-\frac{\delta^2}{24}\mathbf{f}(\mathbf{u})_{xxx}(x_k-\frac{\delta}{2},t^{n-1})+O(\delta^4)\right)\} \\
&\quad +O(\delta^2) \\
&= \frac{1}{\delta^2}\{\mathbf{A}(\mathbf{u}(x_k+\frac{\delta}{2},t^{n-1}))\left(\mathbf{f}(\mathbf{u}(x_{k+1},t^{n-1}))-\mathbf{f}(\mathbf{u}(x_k,t^{n-1}))\right) \\
&\quad -\mathbf{A}(\mathbf{u}(x_k-\frac{\delta}{2},t^{n-1}))\left(\mathbf{f}(\mathbf{u}(x_k,t^{n-1}))-\mathbf{f}(\mathbf{u}(x_{k-1},t^{n-1}))\right)\} \\
&\quad -\frac{\delta}{24}\mathbf{A}(\mathbf{u}(x_k+\frac{\delta}{2},t^{n-1}))\mathbf{f}(\mathbf{u})_{xxx}(x_k+\frac{\delta}{2},t^{n-1})+\frac{\delta}{24}\mathbf{A}(\mathbf{u}(x_k-\frac{\delta}{2},t^{n-1}))\mathbf{f}(\mathbf{u})_{xxx}(x_k-\frac{\delta}{2},t^{n-1}) \\
&\quad +O(\delta^2) \\
&= \frac{1}{\delta^2}\{\left(\frac{\mathbf{A}(\mathbf{u}(x_{k+1},t^{n-1}))+\mathbf{A}(\mathbf{u}(x_k,t^{n-1}))}{2}-\frac{\delta^2}{8}\mathbf{A}(\mathbf{u})_{xx}(x_k,t^{n-1})+O(\delta^3)\right)\left(\mathbf{f}(\mathbf{u}(x_{k+1},t^{n-1}))-\mathbf{f}(\mathbf{u}(x_k,t^{n-1}))\right) \\
&\quad -\left(\frac{\mathbf{A}(\mathbf{u}(x_k,t^{n-1}))+\mathbf{A}(\mathbf{u}(x_{k-1},t^{n-1}))}{2}-\frac{\delta^2}{8}\mathbf{A}(\mathbf{u})_{xx}(x_k,t^{n-1})+O(\delta^3)\right)\left(\mathbf{f}(\mathbf{u}(x_k,t^{n-1}))-\mathbf{f}(\mathbf{u}(x_{k-1},t^{n-1}))\right)\} \\
&\quad -\frac{\delta}{24}\mathbf{A}(\mathbf{u}(x_k,t^{n-1}))\mathbf{f}(\mathbf{u})_{xxx}(x_k,t^{n-1})+\frac{\delta}{24}\mathbf{A}(\mathbf{u}(x_k,t^{n-1}))\mathbf{f}(\mathbf{u})_{xxx}(x_k,t^{n-1})+O(\delta^2) \\
&= \frac{1}{2\delta^2}\{\left(\mathbf{A}(\mathbf{u}(x_{k+1},t^{n-1}))+\mathbf{A}(\mathbf{u}(x_k,t^{n-1}))\right)\left(\mathbf{f}(\mathbf{u}(x_{k+1},t^{n-1}))-\mathbf{f}(\mathbf{u}(x_k,t^{n-1}))\right) \\
&\quad -\left(\mathbf{A}(\mathbf{u}(x_k,t^{n-1}))+\mathbf{A}(\mathbf{u}(x_{k-1},t^{n-1}))\right)\left(\mathbf{f}(\mathbf{u}(x_k,t^{n-1}))-\mathbf{f}(\mathbf{u}(x_{k-1},t^{n-1}))\right)\} \\
&\quad \left(-\frac{1}{8}\mathbf{A}(\mathbf{u})_{xx}(x_k,t^{n-1})+O(\delta)\right)\left(\mathbf{f}(\mathbf{u}(x_{k+1},t^{n-1}))-2\mathbf{f}(\mathbf{u}(x_k,t^{n-1}))+\mathbf{f}(\mathbf{u}(x_{k-1},t^{n-1}))\right) \\
&\quad +O(\delta^2) \\
&= \frac{1}{2\delta^2}\{\left(\mathbf{A}(\mathbf{u}(x_{k+1},t^{n-1}))+\mathbf{A}(\mathbf{u}(x_k,t^{n-1}))\right)\left(\mathbf{f}(\mathbf{u}(x_{k+1},t^{n-1}))-\mathbf{f}(\mathbf{u}(x_k,t^{n-1}))\right) \\
&\quad -\left(\mathbf{A}(\mathbf{u}(x_k,t^{n-1}))+\mathbf{A}(\mathbf{u}(x_{k-1},t^{n-1}))\right)\left(\mathbf{f}(\mathbf{u}(x_k,t^{n-1}))-\mathbf{f}(\mathbf{u}(x_{k-1},t^{n-1}))\right)\} \\
&\quad \left(-\frac{1}{8}\mathbf{A}(\mathbf{u})_{xx}(x_k,t^{n-1})+O(\delta)\right)\left(\delta^2\mathbf{f}(\mathbf{u})_{xx}(x_k,t^{n-1}))+O(\delta^4)\right) \\
&\quad +O(\delta^2) \\
&= \frac{1}{2\delta^2}\{\left(\mathbf{A}(\mathbf{u}(x_{k+1},t^{n-1}))+\mathbf{A}(\mathbf{u}(x_k,t^{n-1}))\right)\left(\mathbf{f}(\mathbf{u}(x_{k+1},t^{n-1}))-\mathbf{f}(\mathbf{u}(x_k,t^{n-1}))\right) \\
&\quad -\left(\mathbf{A}(\mathbf{u}(x_k,t^{n-1}))+\mathbf{A}(\mathbf{u}(x_{k-1},t^{n-1}))\right)\left(\mathbf{f}(\mathbf{u}(x_k,t^{n-1}))-\mathbf{f}(\mathbf{u}(x_{k-1},t^{n-1}))\right)\} \\
&\quad +O(\delta^2)
\end{aligned}
\tag{3-36}
$$

When evaluated at (x_k,t^{n-1}), $(\mathbf{A}(\mathbf{u})\mathbf{b}(\mathbf{u}))_x$ may be represented by the centered difference quotient:

$$
(\mathbf{A}(\mathbf{u})\mathbf{b}(\mathbf{u}))_x(x_k,t^{n-1}) = \frac{1}{2\delta}\{\mathbf{A}(\mathbf{u}(x_{k+1},t^{n-1}))\mathbf{b}(\mathbf{u}(x_{k+1},t^{n-1}))-\mathbf{A}(\mathbf{u}(x_{k-1},t^{n-1}))\mathbf{b}(\mathbf{u}(x_{k-1},t^{n-1}))\}+O(\delta^2). \tag{3-37}
$$

Evaluating (3-26) at (x_k, t^{n-1}) and making use of (3-36), (3-37), and (3-28) gives:

$$\begin{aligned}
\mathbf{u}_{tt}(x_k,t^{n-1}) &= \frac{1}{2\delta^2}\{\left(\mathbf{A}(\mathbf{u}(x_{k+1},t^{n-1}))+\mathbf{A}(\mathbf{u}(x_k,t^{n-1}))\right)\left(\mathbf{f}(\mathbf{u}(x_{k+1},t^{n-1}))-\mathbf{f}(\mathbf{u}(x_k,t^{n-1}))\right)\\
&\quad -\left(\mathbf{A}(\mathbf{u}(x_k,t^{n-1}))+\mathbf{A}(\mathbf{u}(x_{k-1},t^{n-1}))\right)\left(\mathbf{f}(\mathbf{u}(x_k,t^{n-1}))-\mathbf{f}(\mathbf{u}(x_{k-1},t^{n-1}))\right)\}\\
&\quad -\frac{1}{2\delta}\{\mathbf{A}(\mathbf{u}(x_{k+1},t^{n-1}))\mathbf{b}(\mathbf{u}(x_{k+1},t^{n-1}))-\mathbf{A}(\mathbf{u}(x_{k-1},t^{n-1}))\mathbf{b}(\mathbf{u}(x_{k-1},t^{n-1}))\}\\
&\quad -\frac{1}{2\delta}\gamma(\mathbf{u}(x_k,t^{n-1}))\{\mathbf{f}(\mathbf{u}(x_{k+1},t^{n-1}))-\mathbf{f}(\mathbf{u}(x_{k-1},t^{n-1}))\}+\gamma(\mathbf{u}(x_k,t^{n-1}))\mathbf{b}(\mathbf{u}(x_k,t^{n-1}))\\
&\quad +\left[\frac{\delta^2}{6}\gamma(\mathbf{u}(x_k,t^{n-1}))\mathbf{f}(\mathbf{u})_{xxx}(x_k,t^{n-1})+O(\delta^2)\right]\\
&= \frac{1}{2\delta^2}\{\left(\mathbf{A}(\mathbf{u}(x_{k+1},t^{n-1}))+\mathbf{A}(\mathbf{u}(x_k,t^{n-1}))\right)\left(\mathbf{f}(\mathbf{u}(x_{k+1},t^{n-1}))-\mathbf{f}(\mathbf{u}(x_k,t^{n-1}))\right)\\
&\quad -\left(\mathbf{A}(\mathbf{u}(x_k,t^{n-1}))+\mathbf{A}(\mathbf{u}(x_{k-1},t^{n-1}))\right)\left(\mathbf{f}(\mathbf{u}(x_k,t^{n-1}))-\mathbf{f}(\mathbf{u}(x_{k-1},t^{n-1}))\right)\}\\
&\quad -\frac{1}{2\delta}\{\mathbf{A}(\mathbf{u}(x_{k+1},t^{n-1}))\mathbf{b}(\mathbf{u}(x_{k+1},t^{n-1}))-\mathbf{A}(\mathbf{u}(x_{k-1},t^{n-1}))\mathbf{b}(\mathbf{u}(x_{k-1},t^{n-1}))\}\\
&\quad -\frac{1}{2\delta}\gamma(\mathbf{u}(x_k,t^{n-1}))\{\mathbf{f}(\mathbf{u}(x_{k+1},t^{n-1}))-\mathbf{f}(\mathbf{u}(x_{k-1},t^{n-1}))\}+\gamma(\mathbf{u}(x_k,t^{n-1}))\mathbf{b}(\mathbf{u}(x_k,t^{n-1}))\\
&\quad +O(\delta^2).
\end{aligned} \tag{3-38}$$

3.5.2 Lax-Friedrichs Scheme

If $\mathbf{u}$ is thrice differentiable near (x_k, t^n), Taylor's theorem ensures the following representation of $\mathbf{u}(x_k, t^n)$:

$$\mathbf{u}(x_k,t^n) = \mathbf{u}(x_k,t^{n-1}) + \varepsilon\mathbf{u}_t(x_k,t^{n-1}) + \frac{\varepsilon^2}{2}\mathbf{u}_{tt}(x_k,t^{n-1}) + O(\varepsilon^3). \tag{3-39}$$

By Taylor series manipulations, $\mathbf{u}(x_k, t^{n-1})$ may be approximated by the following average:

$$\mathbf{u}(x_k, t^{n-1}) = \frac{1}{2}\left(\mathbf{u}(x_{k+1}, t^{n-1}) + \mathbf{u}(x_{k-1}, t^{n-1})\right) - \frac{\delta^2}{2}\mathbf{u}_{xx}(x_k, t^{n-1}) + O(\delta^4). \tag{3-40}$$

Substituting (3-40) and (3-29) into (3-39) gives:

$$\begin{aligned}\mathbf{u}(x_k, t^n) = {} & \frac{1}{2}(\mathbf{u}(x_{k+1}, t^{n-1}) + \mathbf{u}(x_{k-1}, t^{n-1})) - \frac{\lambda}{2}\{\mathbf{f}(\mathbf{u}(x_{k+1}, t^{n-1})) - \mathbf{f}(\mathbf{u}(x_{k-1}, t^{n-1}))\} \\ & + \varepsilon \mathbf{b}(\mathbf{u}(x_k, t^{n-1})) + \mathbf{E}_{LF},\end{aligned} \tag{3-41}$$

where

$$\begin{aligned}\mathbf{E}_{LF} &= \frac{-\delta^2}{2}\mathbf{u}_{xx}(x_k, t^{n-1}) + \frac{\varepsilon^2}{2}\mathbf{u}_{tt}(x_k, t^{n-1}) - \frac{\varepsilon\delta^2}{6}\mathbf{f}(\mathbf{u})_{xxx}(x_k, t^{n-1}) + O(\varepsilon\delta^4) + O(\delta^4) + O(\varepsilon^3) \\ &= \frac{-\delta^2}{2}\mathbf{u}_{xx}(x_k, t^{n-1}) + \frac{\varepsilon^2}{2}\mathbf{u}_{tt}(x_k, t^{n-1}) + O(\varepsilon\delta^2) + O(\delta^4) + O(\varepsilon^3).\end{aligned} \tag{3-42}$$

Motivated by (3-41), the unsplit LF scheme approximates $\mathbf{u}(x_k, t^n)$ via the formula:

$$\mathbf{u}_k^n = \frac{1}{2}(\mathbf{u}_{k+1}^{n-1} + \mathbf{u}_{k-1}^{n-1}) - \frac{\lambda}{2}\{\mathbf{f}(\mathbf{u}_{k+1}^{n-1}) - \mathbf{f}(\mathbf{u}_{k-1}^{n-1})\} + \varepsilon \mathbf{b}(\mathbf{u}_k^{n-1}). \tag{3-43}$$

The local truncation error of (3-43) is:

$$\boldsymbol{\tau}_k^n \equiv \frac{\mathbf{u}(x_k,t^n)-\mathbf{u}_k^n}{\varepsilon} = \frac{\mathbf{E}_{LF}}{\varepsilon} = \frac{-\delta^2}{2\varepsilon}\mathbf{u}_{xx}(x_k,t^{n-1}) - \frac{\varepsilon}{2}\mathbf{u}_{tt}(x_k,t^{n-1}) + O(\delta^2) + O(\frac{\delta^4}{\varepsilon}) + O(\varepsilon^2). \tag{3-44}$$

Recalling that $\lambda \equiv \frac{\varepsilon}{\delta}$ is assumed to be fixed, (3-44) proves that the local truncation error of the LF scheme is first-order. Expanding (3-26) yields:

$$\begin{aligned}\mathbf{u}_{tt} &= \mathbf{A}^2(\mathbf{u})\mathbf{u}_{xx} + [\mathbf{A}(\mathbf{u})]_x\mathbf{A}(\mathbf{u})\mathbf{u}_x + \mathbf{A}(\mathbf{u})[\mathbf{A}(\mathbf{u})]_x\mathbf{u}_x \\ &\quad -[\mathbf{A}(\mathbf{u})]_x\mathbf{b}(\mathbf{u}) - \mathbf{A}(\mathbf{u})\boldsymbol{\gamma}(\mathbf{u})\mathbf{u}_x - \boldsymbol{\gamma}(\mathbf{u})\mathbf{A}(\mathbf{u})\mathbf{u}_x + \boldsymbol{\gamma}(\mathbf{u})\mathbf{b}(\mathbf{u}).\end{aligned} \tag{3-45}$$

Evaluating (3-45) at (x_k,t^{n-1}) and substituting the resulting expression for $\mathbf{u}_{tt}(x_k,t^{n-1})$ into (3-44) shows that the dominant (i.e. first-order) terms in the local truncation error of the LF scheme depend on the first and second spatial partial derivatives of $\mathbf{u}$.

In light of (3-43) and definitions (3-2), (2-32), and (2-34), the LF scheme for approximating the solution to the transmission line PDEs is:

$$\mathbf{u}_k^n = \begin{pmatrix} I_k^n \\ Q_k^n \end{pmatrix} = \begin{pmatrix} \frac{1}{2}\left(I_{k+1}^{n-1} + I_{k-1}^{n-1}\right) - \frac{\lambda}{2L}\left(v(Q_{k+1}^{n-1}) - v(Q_{k-1}^{n-1})\right) - \frac{\varepsilon R}{L} I_k^{n-1} \\ \frac{1}{2}\left(Q_{k+1}^{n-1} + Q_{k-1}^{n-1}\right) - \frac{\lambda}{2}\left(I_{k+1}^{n-1} - I_{k-1}^{n-1}\right) - \varepsilon G v(Q_k^{n-1}) \end{pmatrix}. \tag{3-46}$$

From (3-44) and (3-45), the local truncation error in the calculation of I_k^n is:

$$
\begin{aligned}
(\tau_I)_k^n = & \left(\frac{-\delta^2}{2\varepsilon} - \frac{\varepsilon}{2L} v'(Q(x_k, t^{n-1}))\right) I_{xx}(x_k, t^{n-1}) \\
& - \frac{\varepsilon}{2}\left(\left(\frac{1}{L} I_x(x_k, t^{n-1}) + \frac{G}{L} v(Q(x_k, t^{n-1}))\right) v''(Q(x_k, t^{n-1})) + \frac{G}{L}\left(v'(Q(x_k, t^{n-1}))\right)^2 + \frac{R}{L^2} v'(Q(x_k, t^{n-1}))\right) Q_x(x_k, t^{n-1}) \\
& - \frac{\varepsilon R^2}{2L^2} I(x_k, t^{n-1}) + O(\delta^2) + O(\frac{\delta^4}{\varepsilon}) + O(\varepsilon^2).
\end{aligned}
\tag{3-47}
$$

Similarly, the local truncation error in the calculation of Q_k^n is:

$$
\begin{aligned}
(\tau_Q)_k^n = & \left(\frac{-\delta^2}{2\varepsilon} - \frac{\varepsilon}{2L} v'(Q(x_k, t^{n-1}))\right) Q_{xx}(x_k, t^{n-1}) \\
& - \frac{\varepsilon}{2L} v''(Q(x_k, t^{n-1}))\left(Q_x(x_k, t^{n-1})\right)^2 - \frac{\varepsilon}{2}\left(\frac{R}{L} + G v'(Q(x_k, t^{n-1}))\right) I_x(x_k, t^{n-1}) \\
& - \frac{\varepsilon G^2}{2} v(Q(x_k, t^{n-1})) v'(Q(x_k, t^{n-1})) + O(\delta^2) + O(\frac{\delta^4}{\varepsilon}) + O(\varepsilon^2).
\end{aligned}
\tag{3-48}
$$

3.5.3 Lax-Wendroff Scheme

If $\mathbf{u}$ is four-times differentiable near (x_k, t^n), Taylor's theorem ensures the following representation of $\mathbf{u}(x_k, t^n)$:

$$
\mathbf{u}(x_k, t^n) = \mathbf{u}(x_k, t^{n-1}) + \varepsilon \mathbf{u}_t(x_k, t^{n-1}) + \frac{\varepsilon^2}{2} \mathbf{u}_{tt}(x_k, t^{n-1}) + \frac{\varepsilon^3}{6} \mathbf{u}_{ttt}(x_k, t^{n-1}) + O(\varepsilon^4) \tag{3-49}
$$

Substituting (3-29) and (3-38) into (3-49) gives:

$$\begin{aligned}\mathbf{u}(x_k,t^n)=&\mathbf{u}(x_k,t^{n-1})-\frac{\lambda}{2}\{\mathbf{f}(\mathbf{u}(x_{k+1},t^{n-1}))-\mathbf{f}(\mathbf{u}(x_{k-1},t^{n-1}))\}+\varepsilon\mathbf{b}(\mathbf{u}(x_k,t^{n-1}))\\&+\frac{\lambda^2}{4}\{\Big(\mathbf{A}(\mathbf{u}(x_{k+1},t^{n-1}))+\mathbf{A}(\mathbf{u}(x_k,t^{n-1}))\Big)\Big(\mathbf{f}(\mathbf{u}(x_{k+1},t^{n-1}))-\mathbf{f}(\mathbf{u}(x_k,t^{n-1}))\Big)\\&-\Big(\mathbf{A}(\mathbf{u}(x_k,t^{n-1}))+\mathbf{A}(\mathbf{u}(x_{k-1},t^{n-1}))\Big)\Big(\mathbf{f}(\mathbf{u}(x_k,t^{n-1}))-\mathbf{f}(\mathbf{u}(x_{k-1},t^{n-1}))\Big)\}\\&-\frac{\varepsilon\lambda}{4}\{\mathbf{A}(\mathbf{u}(x_{k+1},t^{n-1}))\mathbf{b}(\mathbf{u}(x_{k+1},t^{n-1}))-\mathbf{A}(\mathbf{u}(x_{k-1},t^{n-1}))\mathbf{b}(\mathbf{u}(x_{k-1},t^{n-1}))\}\\&-\frac{\varepsilon\lambda}{4}\gamma(\mathbf{u}(x_k,t^{n-1}))\{\mathbf{f}(\mathbf{u}(x_{k+1},t^{n-1}))-\mathbf{f}(\mathbf{u}(x_{k-1},t^{n-1}))\}\\&+\frac{\varepsilon^2}{2}\gamma(\mathbf{u}(x_k,t^{n-1}))\mathbf{b}(\mathbf{u}(x_k,t^{n-1}))+\mathbf{E}_{LW},\end{aligned}\tag{3-50}$$

where

$$\mathbf{E}_{LW}=\frac{\varepsilon^3}{6}\mathbf{u}_{ttt}(x_k,t^{n-1})-\frac{\varepsilon\delta^2}{6}\mathbf{f}(\mathbf{u})_{xxx}(x_k,t^{n-1})+O(\varepsilon\delta^4)+O(\varepsilon^2\delta^2)+O(\varepsilon^4).\tag{3-51}$$

Motivated by (3-50), the unsplit LW scheme approximates $\mathbf{u}(x_k,t^n)$ via the formula:

$$\begin{aligned}\mathbf{u}_k^n=&\mathbf{u}_k^{n-1}-\frac{\lambda}{2}\{\mathbf{f}(\mathbf{u}_{k+1}^{n-1})-\mathbf{f}(\mathbf{u}_{k-1}^{n-1})\}+\varepsilon\mathbf{b}(\mathbf{u}_k^{n-1})\\&+\frac{\lambda^2}{4}\{\Big(\mathbf{A}(\mathbf{u}_{k+1}^{n-1})+\mathbf{A}(\mathbf{u}_k^{n-1})\Big)\Big(\mathbf{f}(\mathbf{u}_{k+1}^{n-1})-\mathbf{f}(\mathbf{u}_k^{n-1})\Big)-\Big(\mathbf{A}(\mathbf{u}_k^{n-1})+\mathbf{A}(\mathbf{u}_{k-1}^{n-1})\Big)\Big(\mathbf{f}(\mathbf{u}_k^{n-1})-\mathbf{f}(\mathbf{u}_{k-1}^{n-1})\Big)\}\\&-\frac{\varepsilon\lambda}{4}\{\mathbf{A}(\mathbf{u}_{k+1}^{n-1})\mathbf{b}(\mathbf{u}_{k+1}^{n-1})-\mathbf{A}(\mathbf{u}_{k-1}^{n-1})\mathbf{b}(\mathbf{u}_{k-1}^{n-1})\}-\frac{\varepsilon\lambda}{4}\gamma(\mathbf{u}_k^{n-1})\{\mathbf{f}(\mathbf{u}_{k+1}^{n-1})-\mathbf{f}(\mathbf{u}_{k-1}^{n-1})\}\\&+\frac{\varepsilon^2}{2}\gamma(\mathbf{u}_k^{n-1})\mathbf{b}(\mathbf{u}_k^{n-1}).\end{aligned}\tag{3-52}$$

The local truncation error of (3-52) is:

$$\boldsymbol{\tau}_k^n \equiv \frac{\mathbf{u}(x_k,t^n)-\mathbf{u}_k^n}{\varepsilon} = \frac{\mathbf{E}_{LW}}{\varepsilon} = \frac{\varepsilon^2}{6}\mathbf{u}_{ttt}(x_k,t^{n-1}) - \frac{\delta^2}{6}\mathbf{f}(\mathbf{u})_{xxx}(x_k,t^{n-1}) + O(\delta^4) + O(\varepsilon\delta^2) + O(\varepsilon^3). \quad (3\text{-}53)$$

Recalling that $\lambda \equiv \frac{\varepsilon}{\delta}$ is assumed to be fixed, (3-53) proves that the local truncation error of the LW scheme is second-order. A laborious calculation, similar to that of (3-45), shows that $\mathbf{u}_{ttt}$ may be expressed in terms of first, second, and third spatial partial derivatives of $\mathbf{u}$. Expanding $\mathbf{f}(\mathbf{u})_{xxx}$ yields:

$$\begin{aligned}
\mathbf{f}(\mathbf{u})_{xxx} &= \left[\mathbf{A}(\mathbf{u})\mathbf{u}_x\right]_{xx} \\
&= \left[\mathbf{A}(\mathbf{u})_x\mathbf{u}_x + \mathbf{A}(\mathbf{u})\mathbf{u}_{xx}\right]_x \\
&= \left[\mathbf{A}(\mathbf{u})_x\mathbf{u}_x\right]_x + \left[\mathbf{A}(\mathbf{u})\mathbf{u}_{xx}\right]_x \\
&= \mathbf{A}(\mathbf{u})_{xx}\mathbf{u}_x + \mathbf{A}(\mathbf{u})_x\mathbf{u}_{xx} + \mathbf{A}(\mathbf{u})_x\mathbf{u}_{xx} + \mathbf{A}(\mathbf{u})\mathbf{u}_{xxx} \\
&= \mathbf{A}(\mathbf{u})\mathbf{u}_{xxx} + 2\mathbf{A}(\mathbf{u})_x\mathbf{u}_{xx} + \mathbf{A}(\mathbf{u})_{xx}\mathbf{u}_x.
\end{aligned} \quad (3\text{-}54)$$

Thus, (3-53) shows that the dominant (i.e. second-order) terms in the local truncation error of the LW scheme depend on the first, second, and third spatial partial derivatives of $\mathbf{u}$.

In light of (3-52) and definitions (3-2), (2-32), and (2-34), the LW scheme for approximating the solution to the transmission line PDEs is:

$$
\begin{aligned}
\mathbf{u}_k^n &= \begin{pmatrix} I_k^n \\ Q_k^n \end{pmatrix} \\
&= \begin{pmatrix} I_k^{n-1} \\ Q_k^{n-1} \end{pmatrix} - \begin{pmatrix} \left(\varepsilon - \dfrac{\varepsilon^2 R}{2L}\right)\left[\dfrac{1}{2\delta L}\left(v(Q_{k+1}^{n-1}) - v(Q_{k-1}^{n-1})\right) + \dfrac{R}{L} I_k^{n-1}\right] \\ \left(\varepsilon - \dfrac{\varepsilon^2 G}{2} v'(Q_k^{n-1})\right)\left[\dfrac{1}{2\delta}\left(I_{k+1}^{n-1} - I_{k-1}^{n-1}\right) + G v(Q_k^{n-1})\right] \end{pmatrix} \\
&\quad + \frac{\lambda^2}{4}\begin{pmatrix} \dfrac{1}{L}\left(v'(Q_{k+1}^{n-1}) + v'(Q_k^{n-1})\right)\left(I_{k+1}^{n-1} - I_k^{n-1}\right) - \dfrac{1}{L}\left(v'(Q_k^{n-1}) + v'(Q_{k-1}^{n-1})\right)\left(I_k^{n-1} - I_{k-1}^{n-1}\right) \\ \dfrac{2}{L}\left(v(Q_{k+1}^{n-1}) - 2v(Q_k^{n-1}) + v(Q_{k-1}^{n-1})\right) \end{pmatrix} \\
&\quad + \frac{\varepsilon\lambda}{4}\begin{pmatrix} \dfrac{G}{L}\left(v(Q_{k+1}^{n-1}) v'(Q_{k+1}^{n-1}) - v(Q_{k-1}^{n-1}) v'(Q_{k-1}^{n-1})\right) \\ \dfrac{R}{L}\left(I_{k+1}^{n-1} - I_{k-1}^{n-1}\right) \end{pmatrix}
\end{aligned}
\tag{3-55}
$$

3.5.4 Hybrid Scheme

By (3-47) and (3-48), the dominant (first-order) terms in the local truncation error of the LF scheme depend on the first and second spatial partial derivatives of $\mathbf{u}$. Based on the previous section, the dominant (second-order) terms in the local truncation error of the LW scheme depend on the first, second, and third spatial partial derivatives of $\mathbf{u}$. Thus, in the vicinity of a steep spatial gradient such as a shock, where the third spatial derivative is large, the LF scheme may be expected to approximate the true solution better than the LW scheme. The hybrid scheme [15] is designed to use the first-order LF scheme where $\mathbf{u}$ contains a steep spatial gradient and to use the second-order LW scheme otherwise. The hybrid scheme achieves this by calculating a weighted average of the LF and LW schemes; the weight assigned to the LW scheme is low where $\mathbf{u}$ contains a steep spatial gradient and high otherwise.

Let $\left(\mathbf{u}_k^n\right)_{LF}$ and $\left(\mathbf{u}_k^n\right)_{LW}$ denote the LF and LW approximations of $\mathbf{u}(x_k,t^n)$ (see (3-43) and (3-52)). Let $\boldsymbol{\alpha}_k^n$ be a diagonal weight matrix that depends upon the spatial smoothness of $\mathbf{u}$ near (x_k,t^n). Then:

$$\begin{aligned}\mathbf{u}(x_k,t^n) &= \boldsymbol{\alpha}_k^n\mathbf{u}(x_k,t^n)+\left(\mathbf{I}-\boldsymbol{\alpha}_k^n\right)\mathbf{u}(x_k,t^n)\\ &= \boldsymbol{\alpha}_k^n\left[\left(\mathbf{u}_k^n\right)_{LW}+\mathbf{E}_{LW}\right]+\left(\mathbf{I}-\boldsymbol{\alpha}_k^n\right)\left[\left(\mathbf{u}_k^n\right)_{LF}+\mathbf{E}_{LF}\right]\\ &= \boldsymbol{\alpha}_k^n\left(\mathbf{u}_k^n\right)_{LW}+\left(\mathbf{I}-\boldsymbol{\alpha}_k^n\right)\left(\mathbf{u}_k^n\right)_{LF}+\boldsymbol{\alpha}_k^n\mathbf{E}_{LW}+\left(\mathbf{I}-\boldsymbol{\alpha}_k^n\right)\mathbf{E}_{LF}\\ &= \mathbf{u}_k^n+\mathbf{E}_H,\end{aligned} \tag{3-56}$$

where

$$\mathbf{u}_k^n = \boldsymbol{\alpha}_k^n\left(\mathbf{u}_k^n\right)_{LW}+\left(\mathbf{I}-\boldsymbol{\alpha}_k^n\right)\left(\mathbf{u}_k^n\right)_{LF} \tag{3-57}$$

and

$$\mathbf{E}_H = \boldsymbol{\alpha}_k^n\mathbf{E}_{LW}+\left(\mathbf{I}-\boldsymbol{\alpha}_k^n\right)\mathbf{E}_{LF}. \tag{3-58}$$

(3-57) is the hybrid formula for calculating an approximation to $\mathbf{u}(x_k,t^n)$. The local truncation error of (3-57) is:

$$\boldsymbol{\tau}_k^n \equiv \frac{\mathbf{u}(x_k,t^n)-\mathbf{u}_k^n}{\varepsilon} = \frac{\mathbf{E}_H}{\varepsilon} = \boldsymbol{\alpha}_k^n\left(\boldsymbol{\tau}_k^n\right)_{LW}+\left(\mathbf{I}-\boldsymbol{\alpha}_k^n\right)\left(\boldsymbol{\tau}_k^n\right)_{LF}, \tag{3-59}$$

where $\left(\boldsymbol{\tau}_k^n\right)_{LW}$ and $\left(\boldsymbol{\tau}_k^n\right)_{LF}$ denote the local truncation errors in the LW and LF approximations (see (3-53) and (3-44)).

The i[th] diagonal entry of the diagonal weighting matrix is given by:

$$\left(\boldsymbol{\alpha}_k^n\right)_i = s\left(\left(\mathbf{r}_k^n\right)_i\right), \tag{3-60}$$

where

$$\left(\mathbf{r}_k^n\right)_i \equiv \frac{\left(\mathbf{u}_k^{n-1}\right)_i - \left(\mathbf{u}_{k-1}^{n-1}\right)_i}{\left(\mathbf{u}_{k+1}^{n-1}\right)_i - \left(\mathbf{u}_k^{n-1}\right)_i}. \tag{3-61}$$

From (3-61), $\left(\mathbf{r}_k^n\right)_i$ differs significantly from unity if $\mathbf{u}_i$ has a steep spatial gradient, a spatial maximum, or spatial minimum near (x_k, t^n); otherwise, $\left(\mathbf{r}_k^n\right)_i$ is close to unity. In (3-60), $s: \mathbb{R} \to [0,1]$ is a function such that:

$$s(r) = \begin{cases} 1 & |r-1| \text{ is small,} \\ 0 & |r-1| \text{ is large.} \end{cases} \tag{3-62}$$

Hence, $\left(\boldsymbol{\alpha}_k^n\right)_i$ is near zero if $\mathbf{u}_i$ has a steep spatial gradient near (x_k, t^n); otherwise, $\left(\boldsymbol{\alpha}_k^n\right)_i$ is close to unity. So, the hybrid approximation given by (3-57) uses the LF scheme to approximate $\mathbf{u}_i(x_k, t^n)$ near a steep spatial gradient and the LW scheme otherwise.

Applying (3-60) and (3-61) to the transmission line PDE problem gives the diagonal weighting matrix for the hybrid scheme:

$$\boldsymbol{\alpha}_k^n = \begin{pmatrix} s\left(\dfrac{I_k^{n-1} - I_{k-1}^{n-1}}{I_{k+1}^{n-1} - I_k^{n-1}}\right) & 0 \\ 0 & s\left(\dfrac{Q_k^{n-1} - Q_{k-1}^{n-1}}{Q_{k+1}^{n-1} - Q_k^{n-1}}\right) \end{pmatrix}. \tag{3-63}$$

Combining (3-57) and (3-63) yields the hybrid scheme for approximating the solution to the transmission line PDEs:

$$\mathbf{u}_k^n = \begin{pmatrix} I_k^n \\ Q_k^n \end{pmatrix} = \begin{pmatrix} s\left(\dfrac{I_k^{n-1} - I_{k-1}^{n-1}}{I_{k+1}^{n-1} - I_k^{n-1}}\right)\left(I_k^n\right)_{LW} + \left[1 - s\left(\dfrac{I_k^{n-1} - I_{k-1}^{n-1}}{I_{k+1}^{n-1} - I_k^{n-1}}\right)\right]\left(I_k^n\right)_{LF} \\ s\left(\dfrac{Q_k^{n-1} - Q_{k-1}^{n-1}}{Q_{k+1}^{n-1} - Q_k^{n-1}}\right)\left(Q_k^n\right)_{LW} + \left[1 - s\left(\dfrac{Q_k^{n-1} - Q_{k-1}^{n-1}}{Q_{k+1}^{n-1} - Q_k^{n-1}}\right)\right]\left(Q_k^n\right)_{LF} \end{pmatrix}. \tag{3-64}$$

SECTION 4

SIMULATION CONDITIONS AND IMPLEMENTATION DETAILS

This section details the modeling and simulation of specific nonlinear transmission lines. The input voltage waveforms injected into these transmission lines are defined and plotted. The transmission line initial conditions (i.e. current and voltage) are given. Physical transmission line properties are stated. Based on the input waveforms and the dielectric properties of the transmission lines, the equations developed in Section 2.3 are used to estimate the position and time of shock wave formation. Finally, specifics of the numerical schemes employed to solve the PDE problem defined by equations (2-28) through (2-30) are presented.

4.1 Input Waveforms and Initial Conditions

The effects of a nonlinear transmission line on both step and pulse input voltage waveforms are simulated. The rising edges of both waveforms are identical. The formula describing the step waveform injected into the input end of the transmission line is:

$$f_1(t) = \begin{cases} 40(1-\cos(\frac{\pi t}{\tau})) \quad \text{V}, & 0 \le t \le \tau, \\ 80 \quad \text{V}, & \tau < t, \end{cases} \quad , \tag{4-1}$$

where $\tau = 2000 * 4 * 10^{-10}$ s. Figure 4-1 plots (4-1). The rise time of (4-1) is 0.4724 μs.

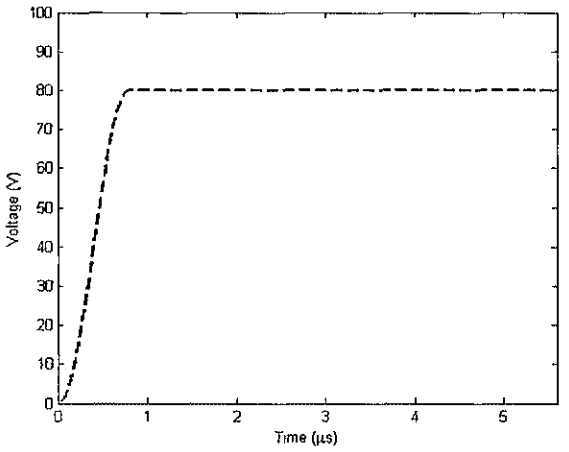

Figure 4-1. Input step waveform.

The formula describing the pulse waveform injected into the input end of the transmission line is:

$$f_2(t)=\begin{cases} 40(1-\cos(\frac{\pi t}{\tau})) \quad \text{V}, & 0\le t\le \tau, \\ 80 \quad \text{V}, & \tau < t \le 2\tau, \\ 40(1-\cos(\frac{\pi(t-\tau)}{\tau})) \quad \text{V}, & 2\tau < t \le 3\tau, \\ 0 \quad \text{V}, & 3\tau < t, \end{cases} \qquad (4\text{-}2)$$

where again $\tau = 2000*4*10^{-10}\text{s}$. Figure 4-2 plots (4-2). Observe that the waveforms prescribed by (4-1) and (4-2) are identical over the interval $[0,2\tau]$. The rise and fall times of (4-2) are both $0.4724\,\mu\text{s}$.

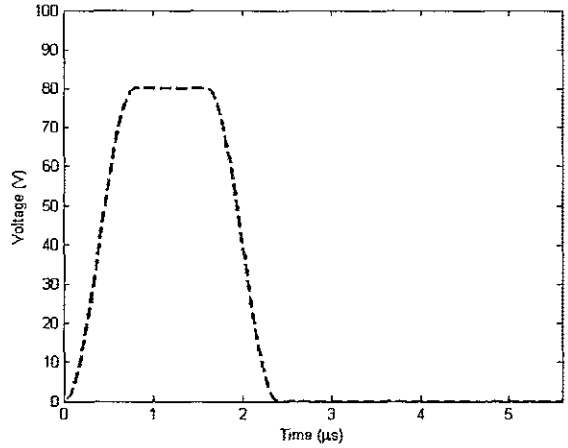

Figure 4-2. Input pulse waveform.

Thus, the left boundary condition (see (2-18)) of the transmission line is:

$$V(0,t) = f_i(t), \qquad t \in (0,\infty), \tag{4-3}$$

where i is either 1 or 2. Under the conservation form transformation, (4-3) is equivalent to the boundary condition (see (2-29)):

$$Q(0,t) = q(f_i(t)) = \tilde{f}_i(t), \tag{4-4}$$

where q is prescribed below in (4-7).

The initial current and voltage (see (2-19)) on the transmission line are assumed to be zero:

$$\begin{cases} I(x,0) = g(x) = 0. \\ V(x,0) = h(x) = 0. \end{cases} \qquad x \in (0,l). \tag{4-5}$$

Under the conservation form transformation, (4-5) is equivalent to the initial conditions (see (2-30)):

$$\begin{cases} I(x,0) = g(x) = \tilde{g}(x) = 0, \\ Q(x,0) = q(h(x)) = \tilde{h}(x) = 0, \end{cases} \qquad x \in (0,l), \tag{4-6}$$

since $q(0) = 0$ for a capacitor.

4.2 Transmission Line Properties

The simulations performed here assume that the transmission line has the following physical properties: the inductance per unit length is $L = 3\mu\text{H/m}$, the resistance per unit length is $R = 0.3\text{m}\Omega\text{/m}$, and the conductance per unit length is $G = 0.5\text{nS/m}$. Transmission lines of the following lengths (in meters) are simulated: 5, 8, 10, 10.5, 11, 12, 15, and 20.

The load resistance at the terminal end of the transmission line is $R_L = 19.9\Omega$. This value of load resistance was observed, based on numerical simulations, to best match (i.e. minimize reflections of) the input waveforms of (4-1) and (4-2). The characteristic impedance of a lossless transmission line ($R = G = 0$) with inductance per

unit length $L = 3\mu H/m$ and capacitance per unit length $C = C(80V) = 5.3430nF/m$ is $Z_0 = \sqrt{\frac{L}{C}} = 23.6956\Omega$. The percent error between Z_0 and R_L is 16%.

The transmission line is assumed to be constructed from a dielectric material called barium strontium titanate (BST). The particular type of BST modeled has the chemical formula $Ba_{0.6}Sr_{0.4}TiO_3$ and a 30μm grain size [16]. Guogang Zhao [16] investigated its dielectric properties by modeling a capacitor consisting of a pair of plates sandwiching this material. He performed numerical simulations to determine the steady-state charge per unit length (q) established on the higher potential plate when a DC voltage source was connected to the capacitor. Zhao performed these simulations for several different DC voltage sources. The odd polynomial extrapolation of Zhao's simulation results yields:

$$q(V) = (-1.7883e-13(\mathrm{Cm^{-1}/V^3}))V^3 + (8.7765e-9(\mathrm{Cm^{-1}/V}))V, \qquad V \in [-128\mathrm{V}, 128\mathrm{V}]. \tag{4-7}$$

A plot of (4-7) is given in Figure 4-3. Observe from Figure 4-3 that q is one-to-one. Note also from (4-7) that q is C^1. As stated in Section 2.2, q therefore possesses a C^1 inverse, v. According to Section 2.2, the existence of such an inverse v for this particular nonlinear transmission line ensures that the transmission line equations ((2-17) through (2-19)) may be cast in conservation form ((2-28) through (2-30)).

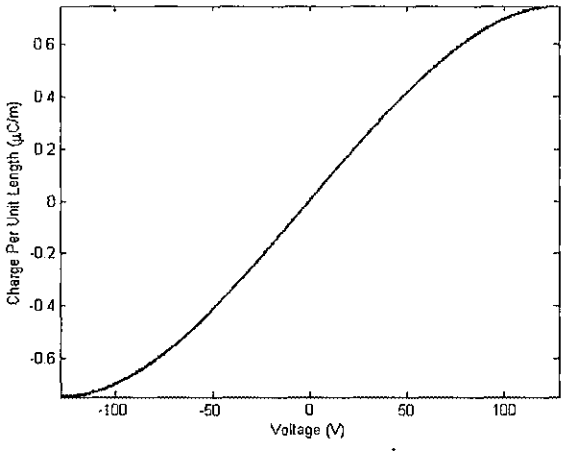

Figure 4-3. A plot of charge per unit length versus voltage.

The capacitance per unit length is defined as $C(V) \equiv \frac{dq(V)}{dV}$. Thus,

$$C(V) = q'(V) = 3*(-1.7883e-13(\mathrm{F/V^2}))V^2 + 8.7765e-9(\mathrm{F}), \quad V \in [-128\mathrm{V}, 128\mathrm{V}] \qquad (4\text{-}8)$$

Figure 4-4 below contains a plot of (4-8). Since q is odd (i.e. $q(-V) = -q(V)$), its derivative C is an even function (i.e. $C(-V) = C(V)$).

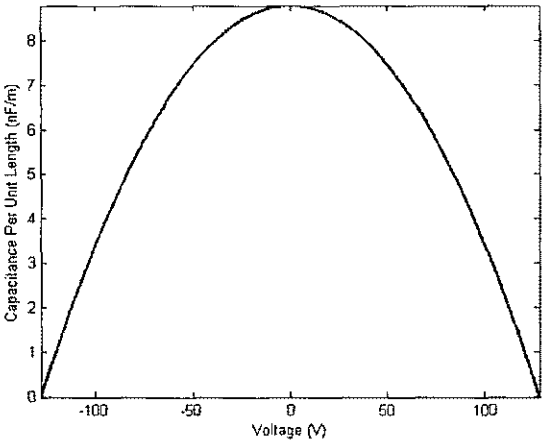

Figure 4-4. A plot of capacitance per unit length versus voltage.

4.3 Shock Formation Location

Assume the input waveform given by either (4-1) or (4-2) is injected into an infinite, nonlinear transmission line with zero initial conditions and the same parameters as those specified in Section 4.2 except that $R = G = 0$. That is, the transmission line is assumed to be infinitely long and lossless. Under these conditions, solving the implicit equation (2-48) yields that $\bar{s} = 0.55394\mu s$; since (4-1) and (4-2) agree on the interval $[0, \tau]$, the solution to (2-48) is the same for both input waveforms. According to equation (2-45), shock formation occurs at time $\bar{t} = 2.0862\mu s$. By equation (2-40), shock formation occurs at position $\bar{x} = 10.8361m$. Thus, the output rise time formula given by equation (2-51) is valid only for transmission lines of length less than $\bar{x} = 10.8361m$. Therefore, shock formation is not expected to occur during the simulation of transmission lines of length (in meters): 5, 8, 10, and 10.5. Shock formation is expected to occur during the simulation of transmission lines of length (in meters): 11, 12, 15, and 20.

4.4 Numerical Scheme Implementation Details

Since $v'(Q) > 0$ for all $Q \in [-.74836\mu C/m, .74836\mu C/m]$, $v'(Q)$ is nonconstant. According to Section 2.2, since $v'(Q)$ is nonconstant, $R \neq 0$, and $G \neq 0$, the transmission line equations in (2-28) describe a 2x2, inhomogeneous, nonlinear, strictly hyperbolic system of balance laws. Thus, the LF, LW, and hybrid numerical schemes described in Section 3 may be applied to solve the PDE problem defined by (2-28) through (2-30).

For a transmission line of length l, the effect of the transmission line on an input waveform is simulated by solving (2-28) through (2-30) with either the LW or hybrid numerical schemes; the LF scheme is not used since it is only first-order accurate. Both the LW and hybrid schemes are implemented by discretizing the spatial-temporal domain $\{(x,t): 0 \le x \le l, 0 \le t \le 5.5996*10^{-6}\text{s}\}$ via the uniform mesh Γ:

$$\Gamma = \{(k\delta, n\varepsilon): k = 0,1,2,...,K-1 \quad n = 0,1,2,...,N-1\}. \tag{4-9}$$

$\delta = 0.05\text{m}$ is the position step, and $\varepsilon = 4*10^{-10}\text{s}$ is the time step. $N = 14000$, and $K = \left\lfloor \frac{l}{\delta} \right\rfloor + 1$ depends on the length of transmission line under consideration.

Using (2-38) and (2-21), the maximum eigenvalue of (2-33) is:

$$\lambda_{\max} = \max_{Q} \sqrt{\frac{v'(Q)}{L}} = \max_{Q} \frac{1}{\sqrt{C(v(Q))L}} = \max_{V} \frac{1}{\sqrt{C(V)L}}. \tag{4-10}$$

The maxima in (4-10) are evaluated over the range of possible values attained by Q and V for this problem ((2-28) through (2-30)). Based on the input waveforms (4-1) and (4-2) and assuming minimal reflections at the terminal end, $V \in [0\text{V}, 80\text{V}]$. Thus,

$$\lambda_{\max} = \max_{V \in [0\text{V},80\text{V}]} \frac{1}{\sqrt{C(V)L}} = \frac{1}{\sqrt{C(80\text{V})L}}. \tag{4-11}$$

So, $\frac{1}{\lambda_{\max}} = \sqrt{C(80\text{V})L} = 1.2661e-7(\text{sm}^{-1})$. Therefore, $\frac{\varepsilon}{\delta} = 8e-9(\text{sm}^{-1}) \le \frac{1}{\lambda_{\max}}$, and so the Courant-Friedrichs-Lewy (CFL) condition [15] is satisfied.

For the hybrid scheme, the switch function described in Section 3.5.4 is defined as:

$$s(r) = \begin{cases} 1 & \frac{1}{2} < r < 2, \\ 0 & r \le \frac{1}{2} \quad \text{or} \quad r \ge 2. \end{cases} \tag{4-12}$$

Thus, the hybrid scheme implemented here evolves the solution using the LW scheme where the solution is smooth and evolves the solution using the LF scheme where the solution is nearly discontinuous.

Note that in order to actually implement any of the schemes described in Section 3, one must be able to calculate $v(Q)$ and $v'(Q)$ for any Q in the range of equation (4-7), i.e. $Q \in [-.74836\mu C/m, .74836\mu C/m]$. Moreover, these calculations must be performed at all KN points in the mesh Γ. The inverse function theorem ensures the existence of an inverse function v of equation (4-7), but it does not indicate how to actually calculate $v(Q)$. Recall however from equation (2-21) that the inverse function theorem does indicate how to calculate $v'(Q)$ provided we know how to calculate $v(Q)$:

$$v'(Q) = \frac{1}{C(v(Q))}. \tag{4-13}$$

Since (4-8) specifies the function C, knowing how to calculate $v(Q)$ is sufficient for implementing the numerical schemes of Section 3.

Given $Q \in [-.74836\mu C/m, .74836\mu C/m]$, calculating $v(Q)$ is equivalent to solving the implicit equation for V:

$$q(V) = Q, \qquad V \in [-128V, 128V] \tag{4-14}$$

Note that solving (4-14) implicitly for V is equivalent to finding the roots of ϕ:

$$\phi(V) = q(V) - Q, \qquad V \in [-128V, 128V] \tag{4-15}$$

Again, we stress that the inverse function theorem guarantees the existence of a unique $V \in [-128\text{V}, 128\text{V}]$ that satisfies (4-14) and that is a root of (4-15). Finding the unique root of (4-15) often requires the use of slow, iterative root finder algorithms (like the Newton-Raphson method [17]) that only yield an approximation to the true solution. Since $v(Q)$ must be calculated at all KN points in the mesh Γ, the accumulation of these approximation errors will quickly negate the accuracy of the LW and hybrid schemes. These approximation errors may be reduced considerably by decreasing the root finder error tolerance, but the decreased tolerance increases the number of iterations performed at each mesh point in Γ, making the overall simulation running time excessive. Thus, we are led to conclude that an analytical formula giving the exact root of equation (4-15) must be developed in order to accurately solve the transmission line equations in reasonable time.

When (4-7) is substituted into (4-15), a cubic polynomial results:

$$\phi(V) = aV^3 + bV + c, \qquad V \in [-128\text{V}, 128\text{V}], \tag{4-16}$$

where $a = -1.7883e-13(\text{Cm}^{-1}/\text{V}^3)$, $b = 8.7765e-9(\text{Cm}^{-1}/\text{V})$, and $c = -Q$. Dividing (4-16) by $-1.7883e-13$ gives another cubic whose unique root agrees with that of (4-16):

$$\tilde{\phi}(V) = \tilde{a}V^3 + \tilde{b}V + \tilde{c}, \qquad V \in [-128\text{V}, 128\text{V}], \tag{4-17}$$

where $\tilde{a} = 1(\text{Cm}^{-1}/\text{V}^3)$, $\tilde{b} = -4.9077e-4(\text{Cm}^{-1}/\text{V})$, and $\tilde{c} = \dfrac{Q}{1.7883e-13}$.

Suppose the domain of (4-17) is extended to include all real numbers:

$$\psi(V) = \tilde{a}V^3 + \tilde{b}V + \tilde{c}, \qquad V \in \mathbb{R}. \tag{4-18}$$

By construction, (4-18) possesses a unique root in the interval $V \in [-128\text{V}, 128\text{V}]$. If $27\tilde{c}^2 + 4\tilde{b}^3 \le 0$, then (4-18) possesses three real roots:

$$T\cos\theta, \qquad T\cos(\theta + \frac{2\pi}{3}), \qquad T\cos(\theta + \frac{4\pi}{3}), \tag{4-19}$$

where T is the positive square root of $\frac{-4\tilde{b}}{3}$ and θ is a solution of $\cos(3\theta) = \frac{-4\tilde{c}}{T^3}$ [18]. Rotman [18] proves the existence of T and θ provided that $27\tilde{c}^2 + 4\tilde{b}^3 \le 0$.

A brief calculation shows that $27\tilde{c}^2 + 4\tilde{b}^3 \le 0 \Leftrightarrow |Q| \le \sqrt{\frac{4b^3}{27|a|}} = .74836\mu\text{C/m}$.

Since $Q \in [-.74836\mu\text{C/m}, .74836\mu\text{C/m}]$ by assumption, $27\tilde{c}^2 + 4\tilde{b}^3 \le 0$. Hence, the unique root of (4-15) may be found quickly and accurately by calculating the three real numbers defined by (4-19) and selecting the unique one that lies in the interval $[-128\text{V}, 128\text{V}]$.

SECTION 5

RESULTS AND DISCUSSION

This section summarizes the numerically simulated effects of a nonlinear transmission line of varying length on step and pulse input voltage waveforms. Both the LW and hybrid numerical schemes were employed in the simulations. This section also briefly investigates the application of the nonlinear transmission line as a pulse generator.

5.1 Step Input Simulations

Simulations were performed to investigate the effect of a nonlinear transmission line on the step input waveform prescribed by (4-1). The transmission line's initial conditions and physical properties are stated in Sections 4.1 and 4.2. Several lengths (in meters) of transmission line were simulated: 5, 8, 10, 10.5, 11, 12, 15, and 20. Recall from Section 4.3 that the estimated shock formation location under these conditions is 10.8361m. Beyond 12.6m, the LW scheme ceases to work because the Gibbs oscillations that occur near the sharp gradient exceed the voltages for which q is defined (please refer to (4-7) and Figures 5-5, 5-7, 5-9, and 5-11). Thus, no LW results are listed in Tables 5-1 or 5-2 for transmission lines of length 15m and 20m.

The propagation time is the time at which a portion of the input step waveform reaches the terminal end of the transmission line. In this thesis, the portion examined is 79.95V (near the 80V maximum amplitude). Table 5-1 compares the expected and simulated propagation times for this portion of the input waveform. The expected

propagation time is calculated by applying equation (2-49). In the last two columns of Table 5-1, the LW propagation times are listed first, while the hybrid propagation times are listed second. The small percent errors between the expected and simulated propagation times indicate that the simulation results may be trusted. Note that the percent errors measured for the LW scheme are always smaller than those measured for the hybrid scheme.

Table 5-2 shows the simulated rise times of the output waveform (i.e. the waveform seen at the terminal end) for each transmission line length. The simulated rise times obtained via the LW scheme are listed first; the simulated rise times obtained via the hybrid scheme are listed second. Observe that the simulated rise times are all less than the input rise time ($0.4724\,\mu s$), illustrating rise time sharpening. Also observe that the simulated rise times decrease as the lengths increase. The expected rise time column of Table 5-2 was calculated for pre-shock formation lengths using equation (2-52). The final column of Table 5-2 compares the expected and simulated output rise times for the pre-shock formation lengths; the small percent errors between these rise times lend credence to the veracity of the numerical simulations. Note that the percent errors measured for the LW scheme tend to be smaller than those measured for the hybrid scheme.

Figures 5-1 through 5-14 show plots of the output waveforms obtained through LW and hybrid numerical simulations for the various transmission line lengths. The sharpening of the step as the transmission line length increases is clearly visible. As the transmission line length approaches the predicted shock formation position (10.8361m), the LW output begins to exhibit Gibbs oscillations near the sharp gradient (see Figures 5-5 and 5-7). Beyond 10.8361m, the Gibbs oscillations in the LW output continue to

increase in amplitude (see Figures 5-9 and 5-11). As previously mentioned, beyond 12.6m, the LW scheme ceases to work because the large Gibbs oscillations exceed the voltages for which (4-7) is defined. In contrast, the hybrid output remains smooth for all transmission line lengths.

Table 5-1. Expected and simulated propagation times for step waveform.

Length (m)	Expected Propagation Time (μs)	Simulated Propagation Time (μs)	Percent Error (%)
5	1.43328	1.4108 / 1.5116	1.57 / 5.46
8	1.813249	1.7892 / 1.8956	1.33 / 4.54
10	2.066561	1.9912 / 2.1764	3.65 / 5.32
10.5	2.129889	2.0588 / 2.2508	3.34 / 5.68
11	2.193217	2.1276 / 2.3180	2.99 / 5.69
12	2.319873	2.2664 / 2.4708	2.30 / 6.51
15	2.699841	- / 2.9344	- / 8.69
20	3.333122	- / 3.7004	- / 11.02

Table 5-2. Expected and simulated output rise times for step waveform.

Length (m)	Expected Output Rise Time (μs)	Simulated Output Rise Time (μs)	Percent Error (%)
5	0.33323	0.3304 / 0.3308	0.85 / 0.73
8	0.249728	0.2492 / 0.2492	0.21 / 0.21
10	0.19406	0.2012 / 0.2132	3.68 / 9.86
10.5	0.180143	0.1904 / 0.2044	5.69 / 13.47
11	-	0.1800 / 0.2004	- / -
12	-	0.1592 / 0.1896	- / -
15	-	- / 0.1632	- / -
20	-	- / 0.1304	- / -

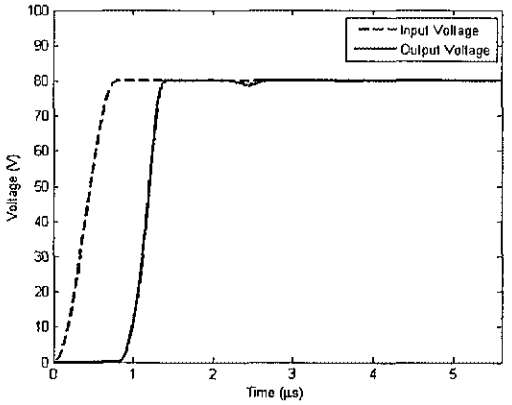

Figure 5-1. LW scheme at 5m.

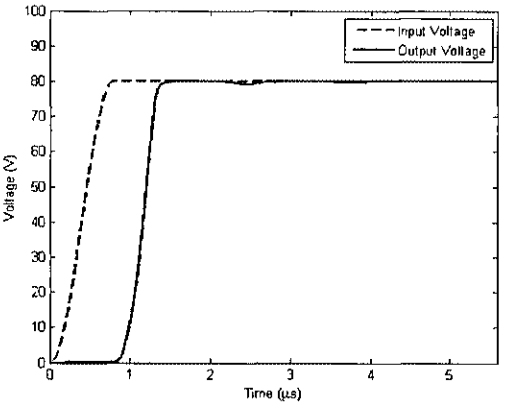

Figure 5-2. Hybrid scheme at 5m.

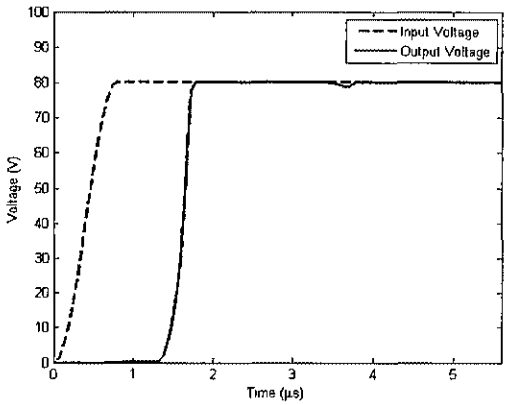

Figure 5-3. LW scheme at 8m.

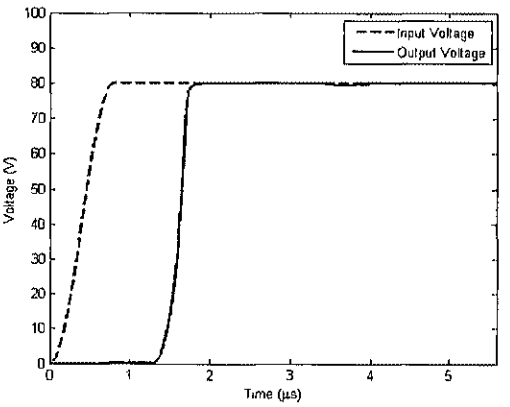

Figure 5-4. Hybrid scheme at 8m.

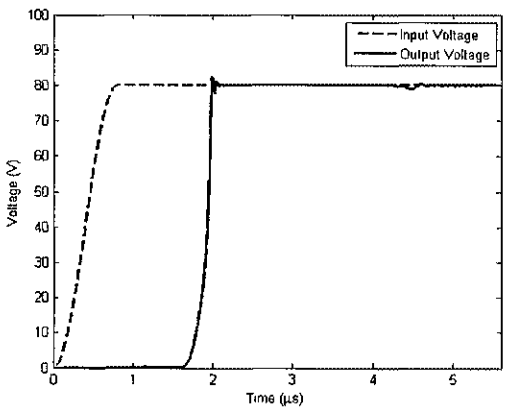

Figure 5-5. LW scheme at 10m.

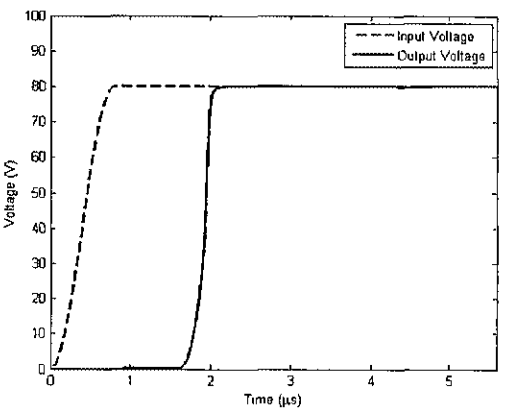

Figure 5-6. Hybrid scheme at 10m.

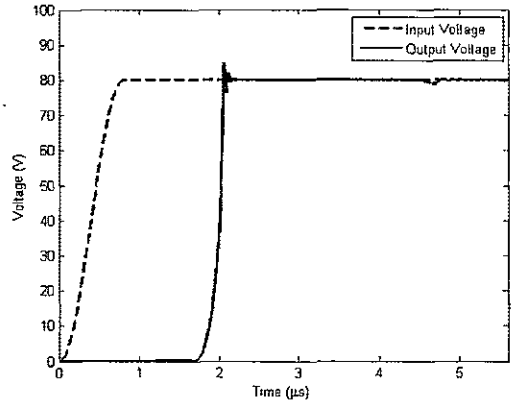

Figure 5-7. LW scheme at 10.5m.

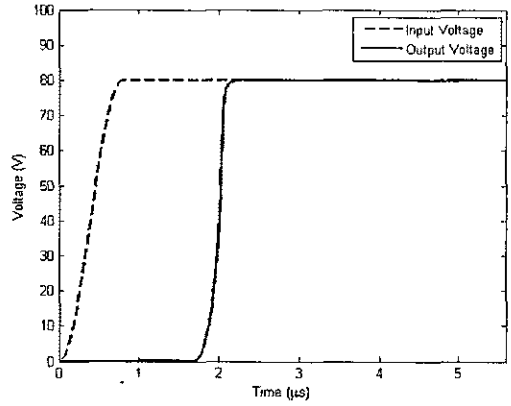

Figure 5-8. Hybrid scheme at 10.5m.

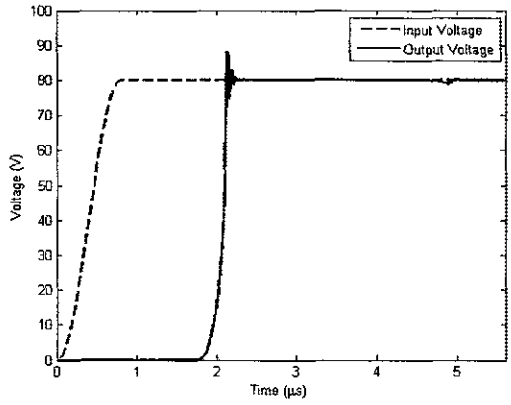

Figure 5-9. LW scheme at 11m.

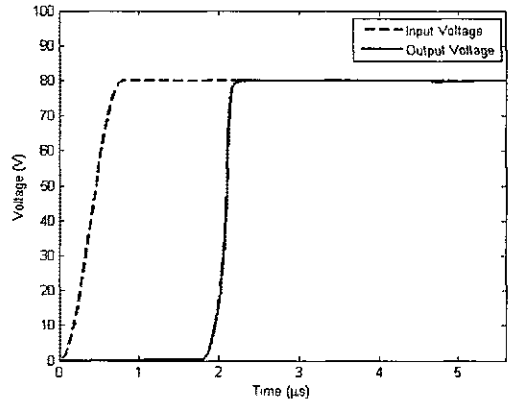

Figure 5-10. Hybrid scheme at 11m.

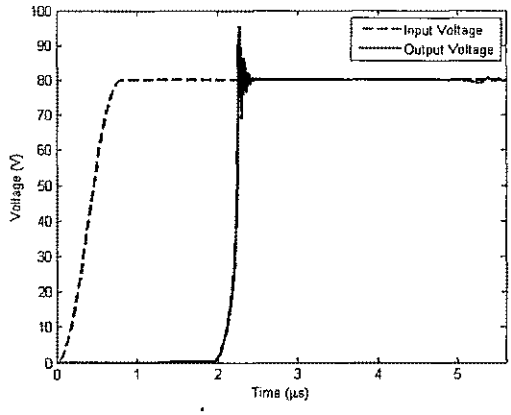

Figure 5-11. LW scheme at 12m.

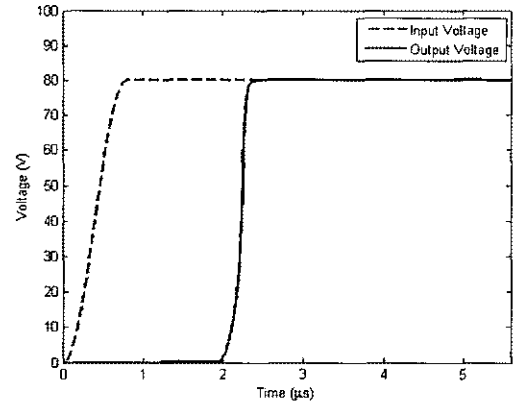

Figure 5-12. Hybrid scheme at 12m.

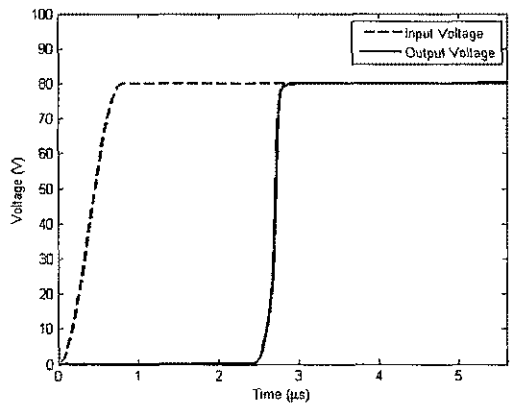

Figure 5-13. Hybrid scheme at 15m.

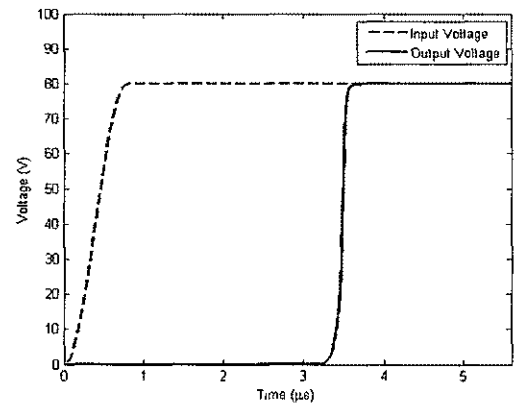

Figure 5-14. Hybrid scheme at 20m.

5.2 Pulse Input Simulations

Simulations were performed to investigate the effect of a nonlinear transmission line on the pulse input waveform prescribed by (4-2). The transmission line's initial conditions and physical properties are stated in Sections 4.1 and 4.2. Several lengths (in meters) of transmission line were simulated: 10, 10.5, 11, and 15. Recall from Section 4.3 that the estimated shock formation location under these conditions is 10.8361m. Beyond

12.6m, the LW scheme ceases to work because the Gibbs oscillations that occur near the sharp rise exceed the voltages for which q is defined (see Section 5.1). Thus, no LW results are listed in Tables 5-3 through 5-5 for the transmission line of length 15m.

Tables 5-3 through 5-5 compare the expected and simulated propagation, rise, and fall times for the waveform obtained at the terminal end. Due to the similarity between the step and pulse waveforms, the propagation and rise times of both output waveforms are very similar for equal transmission line lengths. Like Table 5-2, Table 5-4 shows that the rise times decrease as transmission line length increases. In accordance with the predictions of Section 2.6, Table 5-5 shows that the fall time increases as transmission line lengths increase. The tiny percentage of error between expected and simulated fall times suggests that the simulation results are good approximations to the actual solutions.

Figures 5-15 through 5-21 display plots of the output waveforms obtained through LW and hybrid numerical simulations for the various transmission line lengths. It is graphically evident that the rise time of the output pulse is compressed while the fall time is expanded. Also observe the Gibbs oscillations in the LW output for the transmission line lengths: 10m (Figure 5-15), 10.5m (Figure 5-17), and 11m (Figure 5-19). In contrast, the hybrid output is smooth for all transmission line lengths.

Table 5-3. Expected and simulated propagation times for pulse waveform.

Length (m)	Expected Propagation Time (μs)	Simulated Propagation Time (μs)	Percent Error (%)
10	2.066561	1.9912 / 2.1764	3.66 / 5.32
10.5	2.129889	2.0588 / 2.2508	3.34 / 5.68
11	2.193217	2.1276 / 2.3188	2.99 / 5.73
15	2.699841	- / 2.9148	- / 7.96

Table 5-4. Expected and simulated output rise times for pulse waveform.

Length (m)	Expected Output Rise Time (μs)	Simulated Output Rise Time (μs)	Percent Error (%)
10	0.19406	0.2012 / 0.2132	3.68 / 9.86
10.5	0.180143	0.1904 / 0.2044	5.69 / 13.47
11	-	0.1800 / 0.2000	- / -
15	-	- / 0.1636	- / -

Table 5-5. Expected and simulated output fall times for pulse waveform.

Length (m)	Expected Output Fall Time (μs)	Simulated Output Fall Time (μs)	Percent Error (%)
10	0.75074	0.7428 / 0.7424	1.06 / 1.11
10.5	0.764657	0.7564 / 0.7560	1.08 / 1.13
11	0.778574	0.7700 / 0.7696	1.10 / 1.15
15	0.889911	- / 0.8772	- / 1.43

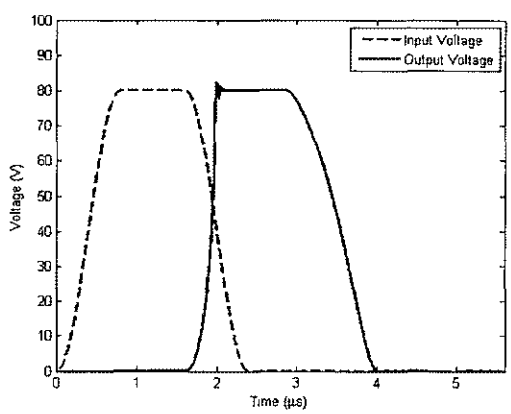

Figure 5-15. LW scheme at 10m.

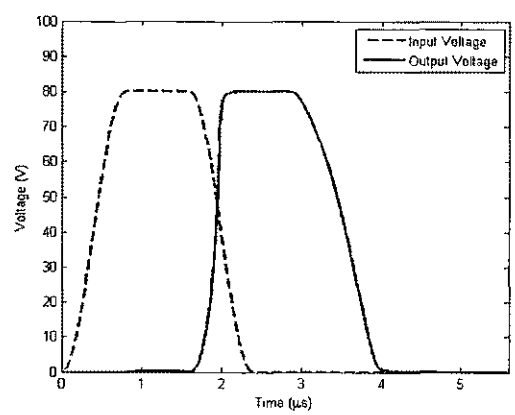

Figure 5-16. Hybrid scheme at 10m.

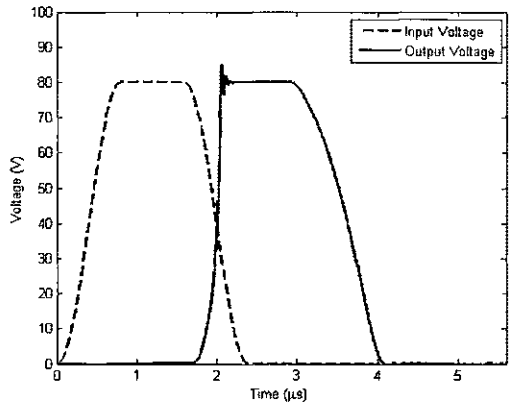

Figure 5-17. LW scheme at 10.5m.

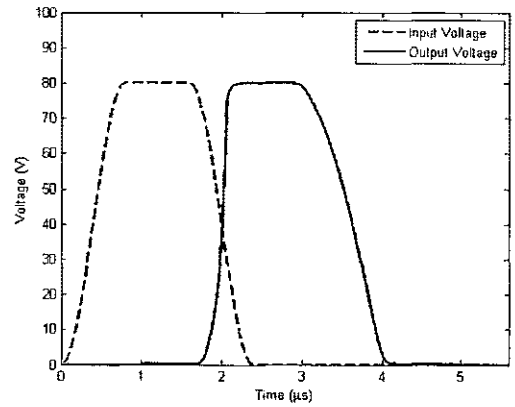

Figure 5-18. Hybrid scheme at 10.5m.

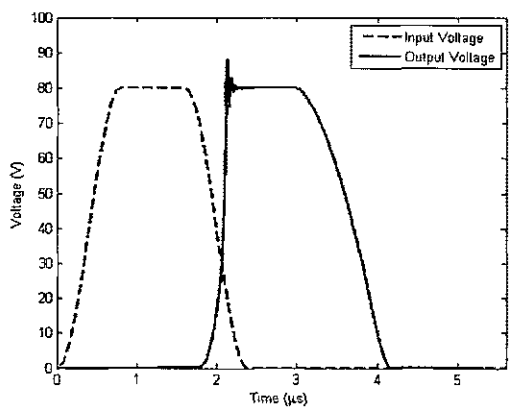

Figure 5-19. LW scheme at 11m.

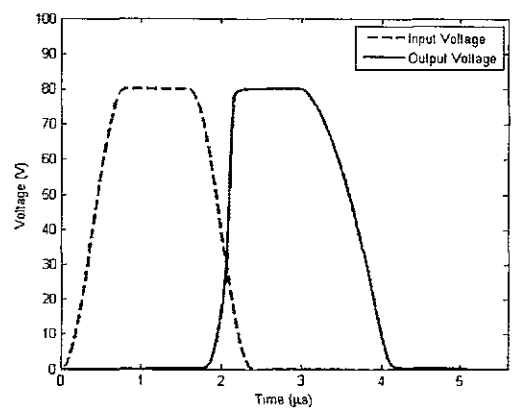

Figure 5-20. Hybrid scheme at 11m.

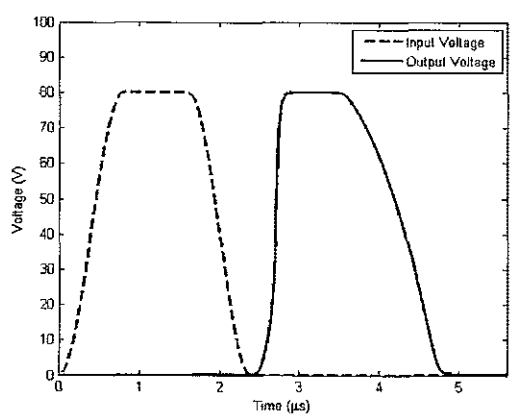

Figure 5-21. Hybrid scheme at 15m.

5.3 Pulse Generator

The nonlinear transmission line may be used to generate high amplitude, short duration voltage pulses by differentiating the output voltage that appears across the terminal resistance. The propagation of the input pulse prescribed by (4-2) has been simulated using the hybrid scheme for several lengths of transmission line: 5m, 10m, 12m, and 15m. In Figures 5-22 through 5-29, the input waveform, the output waveform, and the numerically differentiated output waveform are plotted for each length of transmission line. The numerical derivative is obtained via a centered difference quotient of the output waveform. In practice, the derivative of the voltage that appears across the terminal resistance could be obtained via a passive differentiator (capacitor in series with a resistor) or a differentiating operational amplifier.

The positive pulse of the differentiated output represents the slope of the output waveform's sharply rising edge, whereas the negative pulse represents the slope of the output waveform's gently falling edge. Recall that the full duration at half maximum (FDHM) of a pulse is the duration for which the pulse exceeds half its maximum amplitude. Table 5-6 shows the maximum amplitudes and FDHMs for the positive and negative pulses; in the second and third columns, data for the positive pulse is listed first. Note that the magnitude of the positive pulse increases with length, while the magnitude of the negative pulse decreases with length. Also note that the duration of the positive pulse decreases with length, while the duration of the negative pulse increases with length.

Table 5-6. Maximum amplitudes and FDHMs of differentiated output waveforms.

Length (m)	Maximum Amplitude (MV)	FDHM (μs)
5	259.639 / -125.733	0.2992 / 0.6904
10	742.250 / -109.794	0.0576 / 0.7676
12	870.449 / -105.162	0.0556 / 0.8000
15	958.871 / -99.524	0.0492 / 0.8284

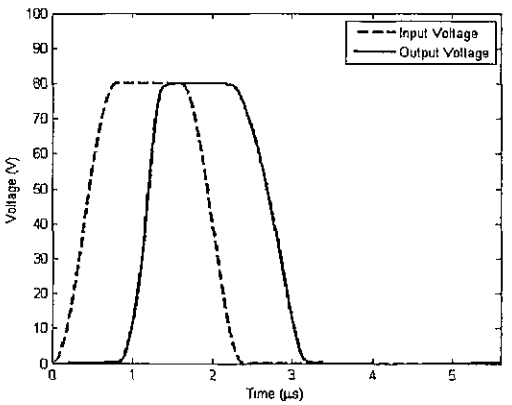

Figure 5-22. Hybrid output at 5m.

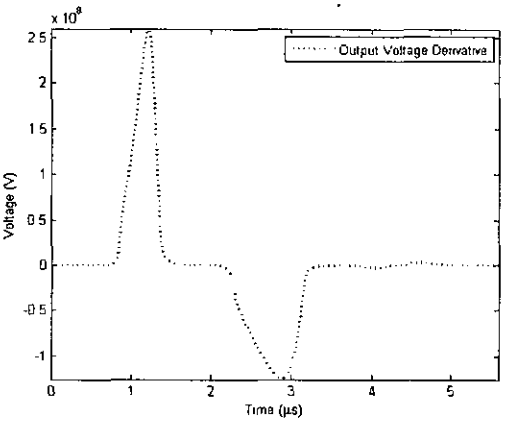

Figure 5-23. Differentiated hybrid output at 5m.

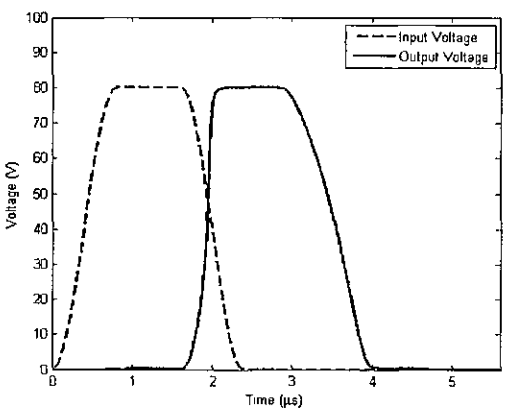

Figure 5-24. Hybrid output at 10m.

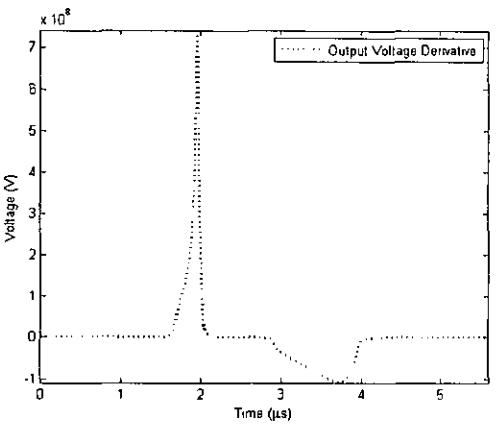

Figure 5-25. Differentiated hybrid output at 10m.

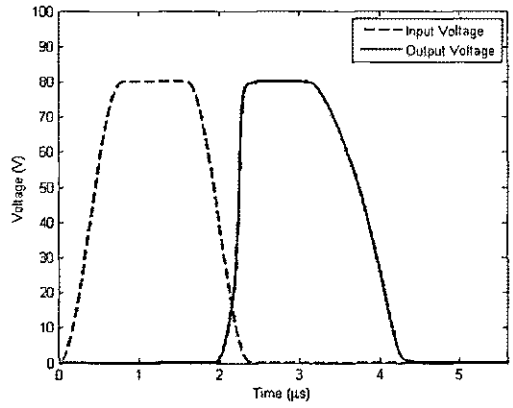

Figure 5-26. Hybrid output at 12m.

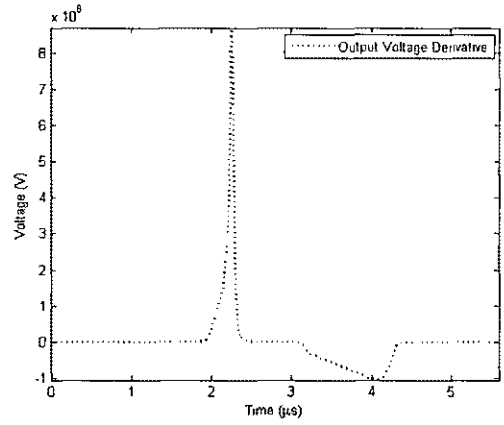

Figure 5-27. Differentiated hybrid output at 12m.

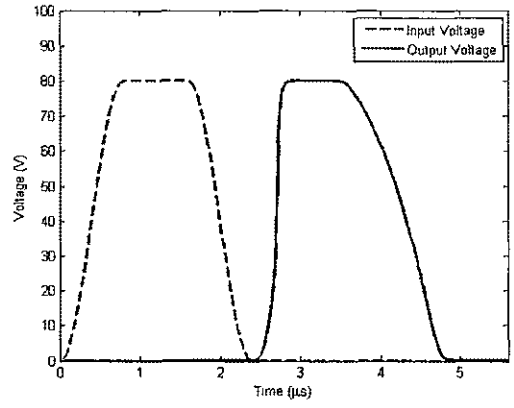

Figure 5-28. Hybrid output at 15m.

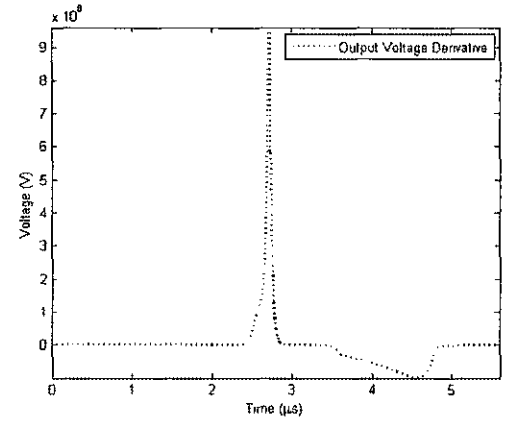

Figure 5-29. Differentiated hybrid output at 15m.

Note that the LW scheme is useless for simulating the pulse generating capabilities of transmission lines exceeding 8-10 meters. As seen in the previous section, the output obtained for such transmission lines exhibit Gibbs oscillations, and the derivative of a waveform with such oscillations possesses multiple spurious positive and negative pulses.

SECTION 6

SUMMARIZING CONCLUSIONS AND FUTURE WORK

6.1 Summarizing Conclusions

This thesis has investigated the numerical solution to the nonlinear partial differential equations that model wave propagation along a nonlinear transmission line with a voltage-dependent capacitance. The equations governing wave propagation along such a transmission line were derived and shown to represent a nonlinear hyperbolic system of balance laws. Three candidate numerical schemes (LF, LW, and hybrid) for solving nonlinear hyperbolic systems of balance laws were derived, analyzed, and applied to the nonlinear telegrapher's equations; two (LW and hybrid) were actually utilized to obtain propagation simulations for several lengths of transmission line. The simulations showed that the temporal slope of rising waveforms increased with propagation distance and that the temporal slope of falling waveforms decreased with propagation distance. The simulation results agreed quite well with theoretical expectations, especially for short transmission lines. As portended by the analysis, the hybrid scheme proved to be superior to the LW scheme for accurately capturing the shock waves that develop in long transmission lines. Finally, the hybrid simulations were used to study and confirm the potential application of a nonlinear transmission line as a pulse generator.

6.2 Suggestions for Future Work

The results obtained from the numerical simulation of nonlinear transmission lines could be compared to physical results obtained by performing experiments on a real nonlinear transmission line. Such a transmission line could be constructed from a series of inductors and carefully tailored voltage-dependent capacitors; the line should be terminated with an appropriate non-reflective, terminal resistance. Physical measurements could be made with an oscilloscope.

Higher-order numerical schemes for solving nonlinear hyperbolic systems of balance laws have and continue to be proposed [1]. Future numerical simulations of nonlinear transmission lines could apply these higher-order schemes to the nonlinear telegrapher's equations in order to obtain more accurate numerical results.

This thesis only considered a nonlinear transmission line having a voltage-dependent capacitance. Future investigations could consider the waveform shaping capabilities of a nonlinear transmission line having both a voltage-dependent capacitance and a current-dependent inductance. It is not difficult to extend the derivation of Section 2.2 to show that the governing equations modeling wave propagation in such a transmission line also represent a nonlinear hyperbolic system of balance laws in terms of magnetic flux per unit length, Φ, and charge per unit length, Q. The nonlinear hyperbolic system of balance laws modeling such a transmission line is:

$$\mathbf{u}_t + \mathbf{f}(\mathbf{u})_x = \mathbf{b}(\mathbf{u}), \tag{6-1}$$

where $\mathbf{u} = \begin{pmatrix} \Phi \\ Q \end{pmatrix}$, $\mathbf{f}(\mathbf{u}) = \begin{pmatrix} v(Q) \\ i(\Phi) \end{pmatrix}$, and $\mathbf{b}(\mathbf{u}) = \begin{pmatrix} -Ri(\Phi) \\ -Gv(Q) \end{pmatrix}$. More complicated nonlinear transmission lines may also be constructed with voltage-dependent capacitances and current-dependent inductances that vary spatially along the line's length.

REFERENCES

[1] R.J. Leveque, *Finite Volume Methods for Hyperbolic Problems*. New York, NY: Cambridge University Press, 2002.

[2] H. Salinger, "Propagation of Telegraph Signals in Krarup Cables." *Archiv. fur Electrotechnik*, vol. 12, pp. 268-285, 1923.

[3] R.B. Riley, "An Analysis of a Nonlinear Transmission Line," Ph.D. dissertation, Dept. Elect. Eng., Stanford University, Palo Alto, CA, 1961.

[4] J.R. Alday, "Narrow Pulse Generation by Nonlinear Transmission Lines," *Proc. IEEE*, p. 739, Jun. 1964.

[5] R. Courant and K.O. Friedrichs, *Supersonic Flow and Shock Waves*. New York: Wiley-Interscience, 1948.

[6] C.M. Dafermos, *Hyperbolic Conservation Laws in Continuum Physics*, 2nd ed. Germany: Springer-Verlag, 2005.

[7] F. Bloom, *Mathematical problems of classical nonlinear electromagnetic theory*. New York: John Wiley & Sons, 1993.

[8] H. Holden and N.H. Risebro, *Front Tracking for Hyperbolic Conservation Laws*. New York: Springer-Verlag, 2002.

[9] J. Johansson and U. Lundgren, "EMC of Transmission Lines," M.S. thesis, Dept. Comp. Sci. and Elect. Eng., Luleå University of Technology, Luleå, Sweden 1997. [Online]. Available: http://www.sm.luth.se/~urban/master/Master/index.html

[10] *Star-HSpice Manual*, Release 2001.2, Avant! Corporation, Fremont, CA, 2001. [Online]. Available: http://www.ece.uci.edu/docs/hspice/hspice_2001_2-269.html

[11] A. Browder, *Mathematical Analysis: An Introduction*. New York: Springer-Verlag, 1996.

[12] L.C. Evans, *Partial Differential Equations*. Providence, RI: American Mathematical Society, 1998.

[13] R.D. Jones, "An Investigation of the Nonlinear Transmission Line," M.S. thesis, Dept. Elect. Eng., University of Pennsylvania, Philadelphia, PA, 1966.

[14] N.S. Nise, *Control Systems Engineering*, 4th ed. Hoboken, NJ: John Wilely & Sons, 2004.

[15] P. Lax, *Hyperbolic Partial Differential Equations*. Providence, RI: American Mathematical Society, 2006.

[16] G. Zhao, "Modeling and Simulations of Electrical Breakdown and Thermal Failure in Zinc Oxide and Titanium Dioxide for High Voltage Dielectric Applications," Ph.D. dissertation, Dept. Elect. Eng., Old Dominion University, Norfolk, VA, 2007.

[17] W.H. Press, S.A. Teukolsky, W.T. Wetterling, and B.P. Flannery, *Numerical Recipes: The Art of Numerical Computing*, 3rd ed. New York, NY: Cambridge University Press, 2007.

[18] J. Rotman, *A First Course in Abstract Algebra*, 2nd ed. Upper Saddle River, NJ: Prentice Hall, 2000.

VITA

Stuart Rogers

Department of Electrical and Computer Engineering

Old Dominion University

Norfolk, VA, 23529

Stuart Rogers received the Sc.B. degrees in mathematics and computer science from Brown University in May 2002. He received the Sc.M. degree in mathematics from Brown University in May 2004. He expects to receive the M.S. degree in electrical engineering from Old Dominion University in May 2008.